SHAPE DESIGN SENSITIVITY ANALYSIS AND OPTIMAL DESIGN OF STRUCTURAL SYSTEMS*

Kyung K. Choi
Department of Mechanical Engineering
and
Center for Computer Aided Design
College of Engineering
The University of Iowa
Iowa City, Iowa 52242

ABSTRACT

The material derivative concept of continuum mechanics and an adjoint variable method of design sensitivity analysis are used to relate variations in structural shape to measures of structural performance. A domain method of shape design sensitivity analysis is used to best utilize the basic character of the finite element method that gives accurate information not on the boundary but in the domain. Implementation of shape design sensitivity analysis using finite element computer codes is discussed. Recent numerical results are used to demonstrate accuracy that can be obtained using the method. Result of design sensitivity analysis is used to carry out design optimization of a built-up structure.

1. INTRODUCTION

A substantial literature has been developed in the field of shape design sensitivity analysis and optimization of structural components [1-3] over the past few years. Contributions to this field have been made using two fundamentally different approaches to structural modeling and analysis. The first approach uses a discretized structural model, based on finite element analysis, and proceeds to carry out shape design sensitivity analysis by controlling finite element node movement and differentiating the algebraic finite element equations [4-6]. The second approach to shape design sensitivity analysis uses an elasticity model of

*Research supported by NASA-Langley Grant NAG-1-215.

the structure and the material derivative method of continuum mechanics to account for changes in shape of the structure [7-13]. Using this approach, expressions for design sensitivity in terms of domain shape change are derived in the continuous setting and evaluated using any available method of structural analysis; e.g., finite element analysis, boundary element analysis, photoelasticity, etc.

Shape design sensitivity analysis for several structural components has been treated in Refs. 2, 9, and 10 where sensitivity information is explicitly expressed as integrals, using integration by parts and boundary and/or interface conditions to obtain identities for transformation of domain integrals to boundary integrals. Numerical calculation of design sensitivity information in terms of the resulting boundary integrals thus requires stresses, strains, and/or normal derivatives of state and adjoint variables on the boundary. However, when the finite element method is used for analysis of built-up structures, the accuracy of numerical results for state and adjoint variables on interface boundaries may not be good [14].

To overcome this difficulty, a domain method of shape design sensitivity analysis is developed in Ref. 15, in which design sensitivity information is expressed as domain integrals, instead of boundary integrals (boundary method). The domain and the boundary methods are analytically equivalent. However, when one uses an approximate numerical method such as finite element analysis, the resulting design sensitivity approximations may give quite different numerical values. Moreover, the domain method offers a remarkable simplification in derivation of shape design sensitivity formulas for built-up structures since interface conditions are not required to obtain shape design sensitivity formulas. In the domain method, numerical evaluation of the sensitivity information is more complicated and inefficient than the result of the boundary method, since the domain method requires integration over the entire domain, whereas the boundary method requires integration over only the variable boundary. To alleviate this problem, a boundary layer of finite elements that vary during the perturbation of the shape of a structural component is introduced in Ref. 16.

In shape design problems, nodal points of the finite element model move as shape changes. In Ref. 17, a method of automatic regridding to account for shape change has been developed using a velocity field in the

domain that obeys the governing deformation equations of the elastic solid.

Using the domain method of Ref. 15 and results of conventional (sizing) design sensitivity analysis theory of Ref. 2, a design component method is developed in Ref. 18 for unified and systematic organization of design sensitivity analysis of built-up structures, with both conventional and shape design variables. That is, conventional and shape design sensitivity formulas for each standard component type can be derived. The result is standard formulas that can be used for design sensitivity analysis of built-up structures, by simply adding contributions from each component. The method gives a systematic organization of computations for design sensitivity analysis that is similar to the way in which computations are organized within a finite element code.

A numerical method has been developed in Ref. 19 to implement the results of the design component method, using the versatility and convenience of existing finite element codes. It is shown in Ref. 19 that calculations can be carried out outside existing finite element codes, using postprocessing data only. Thus, design sensitivity analysis software does not have to be imbedded in an existing finite element code.

The purpose of this paper is to combine these developments to present a unified method of shape design sensitivity analysis and numerical implementation of the method with existing finite element codes. Even though only static response is considered here, the method is also applicable for eigenvalue design sensitivity analysis as shown in Ref. 2.

The design sensitivity analysis method presented here supports optimality criteria method for structural optimization and serves as the foundation for iterative methods of structural optimization using nonlinear programming. At a more practical level, the design sensitivity analysis method can be used to develop an interactive computer-aided design system [2]. A large scale built-up structure is optimized to demonstrate capability of the method.

2. VARIATIONAL FORM OF GOVERNING EQUATIONS

While a substantial library of structural components must be considered to implement the design sensitivity analysis for broad classes of applications, the component library to be considered in this paper is

limited to truss, beam, plate, plane elastic solid, and three dimensional solid components. Even though this is a somewhat restricted class of components, it is general enough that significant applications can be made and practicality of the method can be demonstrated.

In the actual formulation, the truss and beam components, including both bending and torsion of the beam, are incorporated into a single component. Similarly, plate and plane elastic solid components are combined as a single component. To be more specific, the following formation of beam/truss, three dimensional elastic solid, and plate/plane elastic solid components are employed:

A. BEAM/TRUSS

Consider the beam/truss component of Fig. 2.1. The energy bilinear form (internal virtual work) [2] of the component is

$$a_{u,\Omega}(z,\bar{z}) = \int_0^{\ell} EI^1 w^1_{xx} \bar{w}^1_{xx} dx + \int_0^{\ell} EI^2 w^2_{xx} \bar{w}^2_{xx} dx + \int_0^{\ell} GJ\theta_x \bar{\theta}_x dx + \int_0^{\ell} hEv_x \bar{v}_x dx \qquad [2.1]$$

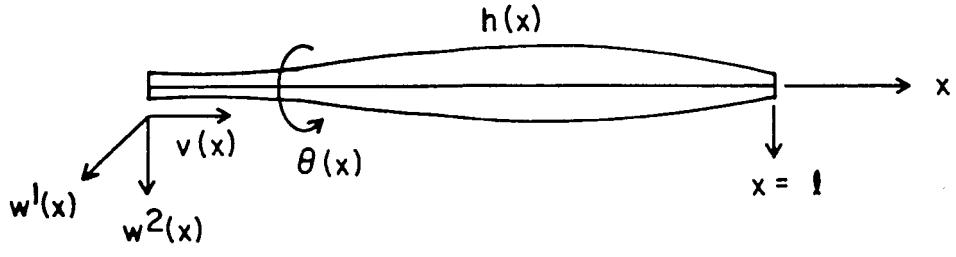

Figure 2.1 Beam/Truss Component

where w^1, w^2, θ, and v are two orthogonal lateral displacements, angle of twist, and axial displacement, respectively, and $z = [w^1, w^2, \theta, v]^T$. Throughout this paper, an overbar; e.g., $\bar{z}$, denotes a virtual displacement. Subscript x in Eq. 2.1 denotes derivative with respect to x. In Eq. 2.1, E, G, I^1, I^2, J, and h are Young's modulus, shear modulus, two moments of inertia, torsional moment of inertia, and cross-sectional area of the component, respectively. The conventional design variable is u = h(x) and the shape design variable is the length of the domain $\Omega = [0,\ell]$. The load linear form (external virtual work) [2] of the component is

$$\ell_{u,\Omega}(\bar{z}) = \int_0^{\ell} q^1\bar{w}^1 dx + \int_0^{\ell} q^2\bar{w}^2 dx + \int_0^{\ell} r\bar{\theta} dx + \int_0^{\ell} f\bar{v} dx \qquad [2.2]$$

where q^1, q^2, r, and f are two orthogonal lateral loads, twisting moment, and axial load, respectively, as shown in Fig. 2.2 [2]. If there are point loads, a Dirac delta measure can be used for q^1, q^2, r, and f in Eq. 2.2 [2].

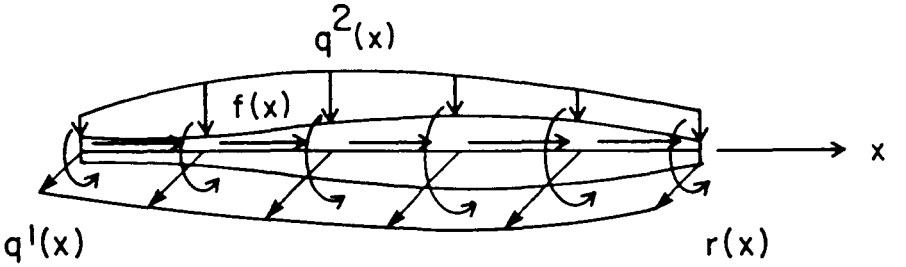

Figure 2.2 External Loads For Beam/Truss

The variational equation of the beam/truss component is [2]

$$a_{u,\Omega}(z,\bar{z}) = \ell_{u,\Omega}(\bar{z}), \qquad \text{for all } \bar{z} \in Z \qquad [2.3]$$

where Z is the space of kinematically admissible displacement. That is, $Z \subset [H^2(0,\ell)]^2 \times [H^1(0,\ell)]^2$ and elements of Z satisfy kinematic boundary conditions where $H^i(0,\ell)$ is the Sobolev space of order i [2]. As possible boundary conditions, the beam/truss component can be simply supported, clamped, cantilevered, or clamped-simply supported. It is shown in Ref. 2 that the variational Eq. 2.3 is applicable for all boundary conditions mentioned.

B. THREE DIMENSIONAL ELASTIC SOLID

Consider the three dimensional elastic solid of Fig. 2.3. For plane elastic solid, results of the three dimensional elastic solid may be reduced.

The strain tensor is defined as

$$\varepsilon^{ij}(z) = \frac{1}{2}(z^i_j + z^j_i), \quad i,j = 1,2,3, \quad x \in \Omega \qquad [2.4]$$

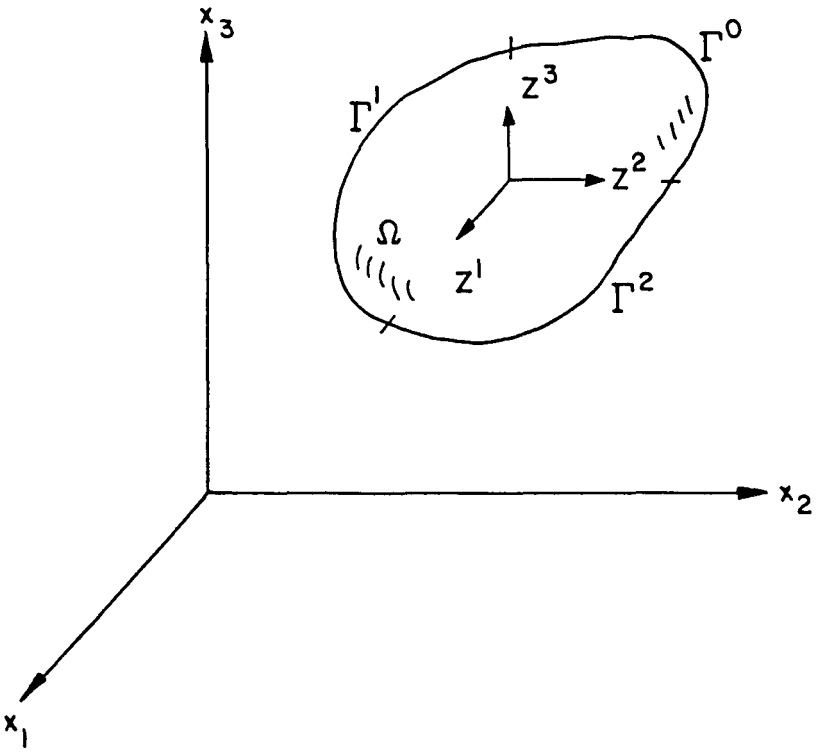

Figure 2.3 Three Dimensional Elastic Solid

where $z = [z^1, z^2, z^3]^T$ is displacement field and subscript i, i = 1,2,3, denotes derivatives with respect to variable x_i. The stress-strain relation (generalized Hooke's Law) is

$$\sigma^{ij}(z) = \sum_{k,\ell=1}^{3} C^{ijk\ell}\varepsilon^{k\ell}(z), \quad i,j,k,\ell = 1,2,3, \quad x \in \Omega \qquad [2.5]$$

where C is the elastic modulus tensor, satisfying symmetry relations $C^{ijk\ell} = C^{jik\ell}$ and $C^{ijk\ell} = C^{ij\ell k}$, i,j,k,ℓ = 1,2,3. The energy bilinear form [2] of the three dimensional elastic solid is

$$a_{u,\Omega}(z,\bar{z}) = \iiint_{\Omega} \left[\sum_{i,j=1}^{3} \sigma^{ij}(z)\varepsilon^{ij}(\bar{z}) \right] d\Omega \qquad [2.6]$$

Even though shape design variable, which is the shape of the domain Ω, is the only design variable in this case, subscript u is left for general treatment. The load linear form [2] of the three dimensional elastic solid is

$$\ell_{u,\Omega}(\bar{z}) = \iiint_{\Omega} [\sum_{i=1}^{3} f^i \bar{z}^i] d\Omega + \iint_{\Gamma^2} [\sum_{i=1}^{3} T^i \bar{z}^i] d\Gamma \qquad [2.7]$$

where Γ^0, Γ^1, and Γ^2 are clamped, traction free, and loaded boundaries, respectively, $f = [f^1, f^2, f^3]^T$ is the body force, and $T = [T^1, T^2, T^3]^T$ is the traction force.

The variational equation of the three dimensional elastic solid is [2]

$$a_{u,\Omega}(z,\bar{z}) = \ell_{u,\Omega}(\bar{z}), \quad \text{for all } \bar{z} \in Z \qquad [2.8]$$

where Z is the space of kinematically admissible displacements; i.e.,

$$Z = \{z \in [H^1(\Omega)]^3 : z^i(x) = 0, \; i = 1, 2, 3, \quad x \in \Gamma^0\} \qquad [2.9]$$

For plane elasticity problems in which either all components of stress in the x_3-direction are zero or all components of strain in the x_3-direction are zero, Eq. 2.8 remains valid, with limits of summation running from 1 to 2 and an appropriate modification of the generalized Hooke's Law of Eq. 2.5.

C. PLATE/PLANE LEASTIC SOLID

Consider the plate/plane elastic solid component of Fig. 2.4. The energy bilinear form [2] of the component is

$$a_{u,\Omega}(z,\bar{z}) = \iint_{\Omega} \hat{D}(t)[(w_{11} + \nu w_{22})\bar{w}_{11} + (w_{22} + \nu w_{11})\bar{w}_{22} + 2(1-\nu)w_{12}\bar{w}_{12}]d\Omega + \iint_{\Omega} t[\sum_{i,j=1}^{2} \sigma^{ij}(v)\varepsilon^{ij}(\bar{v})]d\Omega \qquad [2.10]$$

where $z = [w, v^1, v^2]^T$ is the displacement field. In Eq. 2.10, $\hat{D}(t) = Et^3/[12(1-\nu^2)]$, ν, and t are flexural rigidity, Poisson's ratio, and thickness of the component, respectively. Also, $\sigma^{ij}(v)$ and $\varepsilon^{ij}(v)$ are stress and strain due to an in-plane displacement field $v = [v^1, v^2]^T$, respectively. For this component, the conventional design variable is $u = t(x)$ and the shape design variable is the shape of the domain Ω. The load linear form [2] of the component is

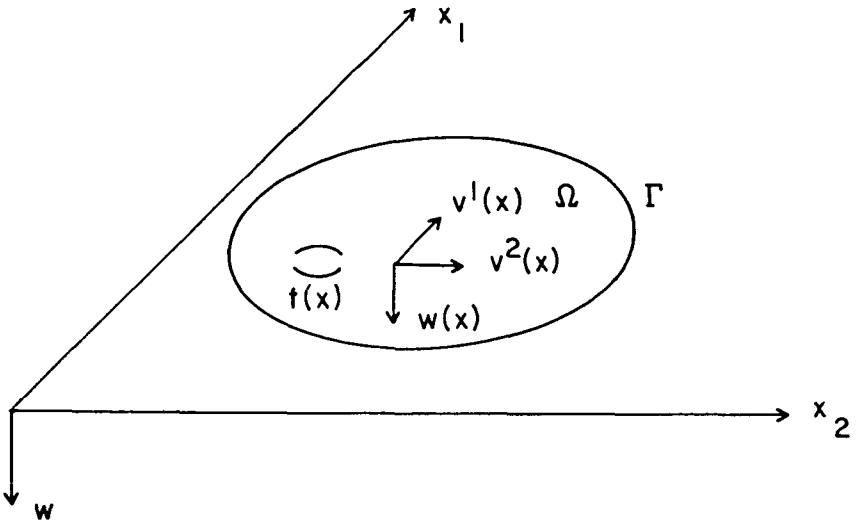

Figure 2.4 Plate/Plane Elastic Solid Component

$$\ell_{u,\Omega}(\bar{z}) = \iint_{\Omega} q\bar{w}d\Omega + \iint_{\Omega} [\sum_{i=1}^{2} f^i\bar{v}^i]d\Omega + \int_{\Gamma^2} [\sum_{i=1}^{2} T^i\bar{v}^i]d\Gamma \qquad [2.11]$$

where q, $f = [f^1, f^2]^T$ and $T = [T^1, T^2]^T$ are lateral load, body force, and traction force, respectively, as shown in Fig. 2.5. As in the beam/truss component, if there are point loads, a Dirac delta measure [2] can be used.

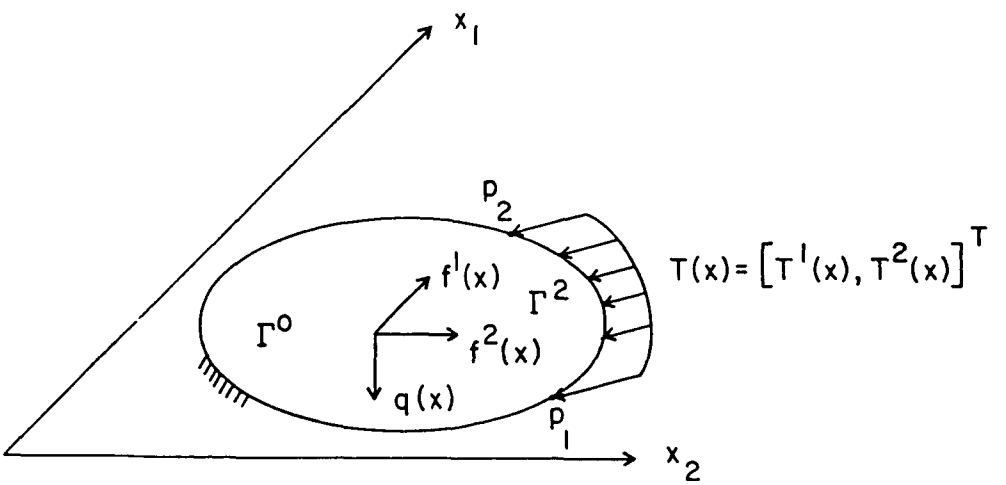

Figure 2.5 External Loads For Plate/Plane Elastic Solid

The variational equation of the plate/plane elastic solid component is [2]

$$a_{u,\Omega}(z,\bar{z}) = \ell_{u,\Omega}(\bar{z}), \qquad \text{for all } \bar{z} \in Z \tag{2.12}$$

where $Z \subset H^2(\Omega) \times [H^1(\Omega)]^2$ and elements of Z satisfy kinematic boundary conditions. For plane leastic solid, kinematic boundary condition is

$$v^i(x) = 0, \quad i = 1,2, \quad x \in \Gamma^0 \tag{2.13}$$

For plate, the boundary can be clamped, simply supported, or free edge. While the calculation may not be as simple as in the case of beam, the variational Eq. 2.12 is valid for all boundary conditions considered [2].

Note that Eqs. 2.3, 2.8, and 2.12, the variational equations for different structural components are all in the same form.

3. MATERIAL DERIVATIVE FOR SHAPE DESIGN SENSITIVITY ANALYSIS

The first step in shape design sensitivity analysis is development of relationships between a variation in shape of a structural component and the resulting variations in functionals that may arise in the shape design problems. Since the shape of domain a structural component occupies is treated as the design variable, it is convenient to think of Ω as a continuous medium and utilize the material derivative idea of continuum mechanics. In this section, the definition of material derivative is introduced and several material derivative formulas that will be used in later sections are derived.

Consider a domain Ω in one, two, or three dimensions, shown schematically in Fig. 3.1. Suppose that only one parameter τ defines the transformation T, as shown in Fig. 3.1. The mapping $T : x \to x_\tau(x)$, $x \in \Omega$, is given by

$$\left.\begin{aligned} x_\tau &= T(x,\tau) \\ \Omega_\tau &\equiv T(\Omega,\tau) \end{aligned}\right\} \tag{3.1}$$

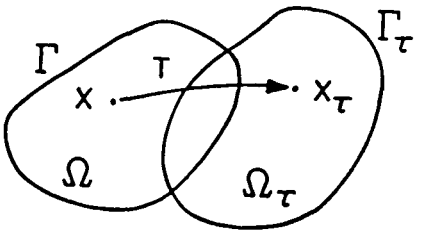

Figure 3.1 One Parameter Family of Mappings

The process of deforming Ω to Ω_τ by the mapping of Eq. 3.1 may be viewed as a dynamic process of deforming a continuum, with τ playing the role of time. At the initial time $\tau = 0$, the domain is Ω. Trajectories of points $x \in \Omega$, beginning at $\tau = 0$, can now be followed. The initial point moves to $x_\tau = T(x,\tau)$. Thinking of τ as time, a design velocity can be defined as

$$V(x_\tau,\tau) \equiv \frac{dx_\tau}{d\tau} = \frac{\partial T(x,\tau)}{\partial \tau} \qquad [3.2]$$

In a neighborhood of $\tau = 0$, under reasonable regularity hypotheses [2],

$$T(x,\tau) = T(x,0) + \tau \frac{\partial T}{\partial \tau}(x,0) + O(\tau^2)$$

$$= x + \tau V(x,0) + O(\tau^2)$$

Ignoring higher order terms,

$$T(x,\tau) = x + \tau V(x) \qquad [3.3]$$

where $V(x) \equiv V(x,0)$. In this paper, only the transformation T of Eq. 3.2 will be considered, the geometry of which is shown in Fig. 3.2. Variations of the domain Ω by the design velocity field $V(x)$ are denoted as $\Omega_\tau = T(\Omega,\tau)$ and the boundary of Ω_τ is denoted as Γ_τ. Henceforth in the paper, the term "design velocity" will be referred to simply as "velocity".

Let Ω be a C^k-regular open set; i.e., its boundary Γ is closed and bounded and can be locally represented by a C^k-function. Let $V(x) \in R^n$ in Eq. 3.2 be a vector defined on a neighborhood U of the closure $\overline{\Omega}$ of Ω

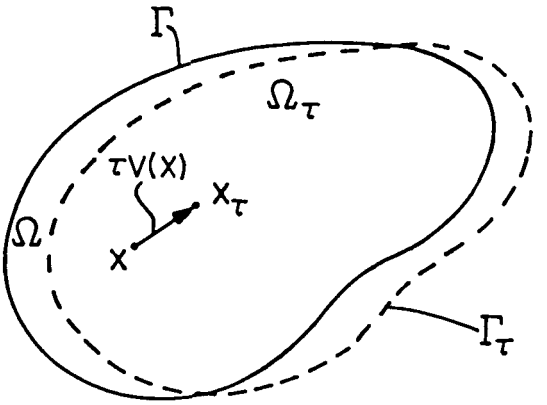

Figure 3.2 Variation of Domain

and $V(x)$ and its derivatives up to order $k > 1$ be continuous. With these hypotheses, it has been shown [20] that for small τ, $T(x,\tau)$ is a homeomorphism (a one-to-one, continuous map with a continuous inverse) from U to $U_\tau \equiv T(U,\tau)$ and that $T(x,\tau)$ and its inverse mapping $T^{-1}(x_\tau,\tau)$ have C^k-regularity and Ω_τ has C^k-regularity.

Suppose $z_\tau(x_\tau)$ is a smooth solution of the elasiticity equations. Then the mapping $z_\tau(x_\tau) \equiv z_\tau(x + \tau V(x))$ is defined on Ω and $z_\tau(x_\tau)$ depends on τ in two ways. First, it is the solution of the boundary-value problem on Ω_τ. Second, it is evaluated at a point x_τ that moves with τ. The pointwise material derivative (which is shown to exist in Ref. 2) at $x \in \Omega$ is defined as

$$\dot{z}(x) = \frac{d}{d\tau} z_\tau(x+\tau V(x))\Big|_{\tau=0} = \lim_{\tau\to 0} \frac{z_\tau(x + \tau V(x)) - z(x)}{\tau} \qquad [3.4]$$

If z_τ has a regular extension to a neighborhood U_τ of $\bar{\Omega}_\tau$, then

$$\dot{z}(x) = z'(x) + \nabla z^T V(x) \qquad [3.5]$$

where

$$z'(x) \equiv \lim_{\tau\to 0} \frac{z_\tau(x) - z(x)}{\tau} \qquad [3.6]$$

is the partial derivative of z.

One attractive feature of the partial derivative is that, with reasonable smoothness assumptions, it commutes with the derivatives with respect to x_i [2]; i.e.,

$$(\frac{\partial z}{\partial x_i})' = \frac{\partial}{\partial x_i}(z') \quad , \quad i = 1,2,3 \qquad [3.7]$$

A pair of technical material derivative formulas that are used throughout the remainder of the paper are summarized in this section. Their proofs are presented in Ref. 2.

Lemma 3.1: Let ψ_1 be a domain functional, defined as an integral over Ω_τ,

$$\psi_1 = \iint_{\Omega_\tau} f_\tau(x_\tau)\, d\Omega_\tau \qquad [3.8]$$

where f_τ is a regular function defined on Ω_τ. If Ω has C^k-regularity, then the material derivative of ψ_1 at Ω is

$$\psi_1' = \iint_\Omega f'(x)d\Omega + \int_\Gamma f(x)\,(V^T n)\, d\Gamma \qquad [3.9]$$

or, equivalently,

$$\psi_1' = \iint_\Omega [f'(x) + \nabla f(x)^T V(x) + f(x)\,\mathrm{div}\, V(x)]d\Omega \qquad [3.10]$$

It is interesting and important to note that only the normal component $(V^T n)$ of the boundary velocity appearing in Eq. 3.9 is needed to account for the effect of domain variation. In fact, it is shown by Theorem 3.5.2 of Ref. 2 that if a general domain functional ψ has a gradient at Ω and if Ω has C^{k+1}-regularity, then only the normal component $(V^T n)$ of the velocity field on the boundary is needed for derivative calculations.

In contrast to Eq. 3.9, use of the mathematically equivalent result given in Eq. 3.10 requires that the velocity field $V(x)$ be defined throughout the domain Ω. Of course, it must be consistent with $(V^T n)$ on Γ. Nevertheless, there are an infinite number of velocity fields that satisfy this condition, for each of which the result of Eqs. 3.9 and 3.10 must be the same.

Next, consider a functional defined as an integration over Γ_τ,

$$\psi_2 = \int_{\Gamma_\tau} g_\tau(x_\tau)\, d\Gamma_\tau \qquad [3.11]$$

Lemma 3.2: Suppose g_τ in Eq. 3.11 is a regular function defined on Γ_τ. If Ω is C^{k+1} regular, the material derivative of ψ_2 is

$$\psi_2' = \int_\Gamma [g'(x) + (\nabla g^T n + H\, g(x))\,(V^T n)]\, d\Gamma \qquad [3.12]$$

where H is the curvatue of Γ in R^2 and twice the mean curvature in R^3.

4. ADJOINT VARIABLE FORMULATION OF SHAPE DESIGN SENSITIVITY ANALYSIS

As seen in Section 3, the static response of a structure depends on the shape of the domain. Existence of the material derivative $\dot{z}$, which is proved in Ref. 2, and material derivative formulas presented in Section 3 are used in this section to derive an adjoint variable method for design sensitivity analysis of several functionals. Since the finite element method is used for numerical analysis of the structural systems in this paper, only the domain method of shape design sensitivity analysis is presented in this section.

The variational equations of several structural components of Eqs. 2.3, 2.8, and 2.12 on a deformed domain, is of the form

$$a_{u,\Omega_\tau}(z_\tau, \bar{z}_\tau) \equiv \iint_{\Omega_\tau} c(z_\tau, \bar{z}_\tau)\, d\Omega_\tau$$
$$= \iint_{\Omega_\tau} f^T \bar{z}_\tau d\Omega_\tau + \int_{\Gamma_{2\tau}} T^T \bar{z}_\tau d\Gamma_\tau \equiv \ell_{u,\Omega_\tau}(\bar{z}_\tau), \quad \text{for all } \bar{z}_\tau \in Z_\tau \qquad [4.1]$$

where Z_τ is the space of kinematically admissible displacements on Ω_τ and $c(\cdot,\cdot)$ is a bilinear mapping that is defined by the integrand of Eqs. 2.1, 2.6, and 2.10.

Taking the material derivative of both sides of Eq. 4.1, using Eqs. 3.10 and 3.11 and noting that the partial derivatives with respect to τ and x commute,

$$[a_{u,\Omega}(z,\bar{z})]' \equiv a'_{u,V}(z,\bar{z}) + a_{u,\Omega}(\dot{z},\bar{z}) = \ell'_{u,V}(\bar{z}), \quad \text{for all } \bar{z} \in Z \qquad [4.2]$$

where, using Eq. 3.5,

$$[a_{u,\Omega}(z,\bar{z})]' = \iint_{\Omega}[c(z,\bar{z}') + c(z',\bar{z}) + \nabla c(z,\overline{z})^{T}V + c(z,\overline{z})\text{div } V]\, d\Omega$$

$$= \iint_{\Omega}[c(z,\dot{\bar{z}} - \nabla\bar{z}^{T}V) + c(\dot{z} - \nabla z^{T}V,\bar{z}) + \nabla c(z,\overline{z})^{T}V$$

$$+ c(z,\overline{z})\text{div } V]\, d\Omega \qquad [4.3]$$

and

$$\ell'_{u,V}(\bar{z}) = \iint_{\Omega}[f^{T}\bar{z}' + \nabla(f^{T}\bar{z})^{T}V + f^{T}\bar{z}\text{div } V]d\Omega$$

$$+ \int_{\Gamma^2}[T^{T}\bar{z}' + (\nabla(T^{T}\bar{z})^{T}n + HT^{T}\bar{z})(V^{T}n)]d\Gamma$$

$$= \iint_{\Omega}[f^{T}(\dot{\bar{z}} - \nabla\bar{z}^{T}V) + \nabla(f^{T}\bar{z})^{T}V + f^{T}\bar{z}\text{div } V]d\Omega$$

$$+ \int_{\Gamma^2}[T^{T}(\dot{\bar{z}} - \nabla\bar{z}^{T}V) + (\nabla(T^{T}\bar{z})^{T}n + HT^{T}\bar{z})(V^{T}n)]d\Gamma \qquad [4.4]$$

The fact that the partial derivatives of the coefficients, which depend on cross-sectional area and thickness, in the bilinear mapping $c(\cdot,\cdot)$ are zero has been used in Eq. 4.3 and $f' = T' = 0$ has been used in Eq. 4.4. For boundary variations, it is supposed that the boundary $\Gamma = \Gamma^0 \cup \Gamma^1 \cup \Gamma^2$ is varied, except that the curve $\partial\Gamma^2$ that bounds the loaded surface Γ^2 is fixed for three dimensional elastic solid, so the velocity field V at $\partial\Gamma^2$ is zero. For the case in which $\partial\Gamma^2$ is not fixed, variation of the traction term in Eq. 4.1 (given as an integral over Γ^2) gives an additional term that was not discussed in lemmas. For this case, the interested reader is referred to Ref. 21. For plane elastic solid component case, these additional terms will be given in Section 5.

For $\bar{z}_\tau$, select $\bar{z}_\tau(x + \tau V(x)) = \bar{z}(x)$; i.e., choose $\bar{z}$ as constant on the line $x_\tau = x + \tau V(x)$. Then, since $H^m(\Omega)$ is preserved by $T(x,\tau)$ (homeomorphism property noted in Section 3), if $\bar{z}$ is an arbitrary element of $H^m(\Omega)$ that satisfies kinematic boundary conditions on Γ, $\bar{z}_\tau$ is an arbitrary element of $H^m(\Omega_\tau)$ that satisfies kinematic boundary conditions on Γ_τ. In this case, using Eq. 3.5,

$$\dot{\bar{z}} = \bar{z}' + \nabla\bar{z}^{T}V = 0 \qquad [4.5]$$

From Eqs. 4.2, 4.3, and 4.4, using Eq. 4.5,

$$a'_{u,V}(z,\bar{z}) = \iint_\Omega [-c(z,\nabla\bar{z}^T V) - c(\nabla z^T V,\bar{z}) + \nabla c(z,\bar{z})^T V + c(z,\bar{z})\text{div } V]d\Omega \quad [4.6]$$

and

$$\ell'_{u,V}(\bar{z}) = \iint_\Omega [\bar{z}^T(\nabla f^T V) + f^T\bar{z}\text{div } V]d\Omega + \int_{\Gamma_2} [-T^T(\nabla\bar{z}^T V) + (\nabla(T^T\bar{z})^T n + HT^T\bar{z})(V^T n)]d\Gamma \quad [4.7]$$

Then, Eq. 4.2 can be rewritten to provide the result

$$a_{u,\Omega}(\dot{z},\bar{z}) = \ell'_{u,V}(\bar{z}) - a'_{u,V}(z,\bar{z}), \qquad \text{for all } \bar{z} \in Z \quad [4.8]$$

Consider a displacement functional that defines the displacement at nodal point $\hat{x} \in \Omega$

$$\psi_1 = z(\hat{x}) = \iint_\Omega \hat{\delta}(x-\hat{x})z(x)d\Omega \quad [4.9]$$

where $\hat{\delta}(x)$ is the Dirac delta measure at the origin. Taking the first variation of Eq. 4.9, using the material derivative,

$$\psi'_1 = \dot{z}(\hat{x}) = \iint_\Omega \hat{\delta}(x-\hat{x})\dot{z}(x)d\Omega \quad [4.10]$$

The objective now is to obtain an explicit expression for ψ'_1 in terms of the velocity field V, which requires eliminating $\dot{z}$. An adjoint equation is introduced by replacing $\dot{z} \in Z$ in Eq. 4.10 by a virtual displacement $\bar{\lambda} \in Z$ and equating terms involving $\bar{\lambda}$ to the energy bilinear form, yielding the adjoint equation for the adjoint variable λ,

$$a_{u,\Omega}(\lambda,\bar{\lambda}) = \iint_\Omega \hat{\delta}(x-\hat{x})\bar{\lambda}(x)d\Omega, \qquad \text{for all } \bar{\lambda} \in Z \quad [4.11]$$

Denote the solution of Eq. 4.11 as $\lambda^{(1)}$.

To take advantage of the adjoint equation, evaluate Eq. 4.11 at $\bar{\lambda} = \dot{z}$, since $\dot{z} \in Z$ [2], to obtain the expression

$$a_{u,\Omega}(\lambda^{(1)},\dot{z}) = \iint_{\Omega} \hat{\delta}(x-\hat{x})\dot{z}(x)d\Omega \qquad [4.12]$$

Similarly, evaluate the identity of Eq. 5.8 at $\bar{z} = \lambda^{(1)}$, since both are in Z, to obtain

$$a_{u,\Omega}(\dot{z},\lambda^{(1)}) = \ell'_{u,V}(\lambda^{(1)}) - a'_{u,V}(z,\lambda^{(1)}) \qquad [4.13]$$

Recalling that the energy bilinear form $a_{u,\Omega}(\cdot,\cdot)$ is symmetric in its arguments, the left sides of Eqs. 4.12 and 4.13 are equal, so

$$\iint_{\Omega} \hat{\delta}(x-\hat{x})\dot{z}(x)d\Omega = \ell'_{u,V}(\lambda^{(1)}) - a'_{u,V}(z,\lambda^{(1)}) \qquad [4.14]$$

Using Eqs. 4.14, Eq. 4.10 yields

$$\psi'_1 = \ell'_{u,V}(\lambda^{(1)}) - a'_{u,V}(z,\lambda^{(1)}) \qquad [4.15]$$

Explicit expressions of the terms in Eq. 4.15, for each structural component can be obtained using Eqs. 4.6 and 4.7. These explicit expressions will be derived in Section 5. This order of presentation was chosen to show basic idea of the adjoint variable method without complicate derivation of expressions.

Note that evaluation of the design sensitivity formula of Eq. 4.15 requires solution of Eq. 4.1 for z. Similarly, Eq. 4.11 must be solved for the adjoint variable $\lambda^{(1)}$. This is an efficient calculation, using finite element analysis, if the boundary-value problem for z has already been solved, requiring only evaluation of the solution of the same set of finite element equations with different right side, called an adjoint load.

Next, consider a locally averaged stress functional over a test volume Ω_p of the three dimensional elastic solid,

$$\psi_2 = \iiint_{\Omega} g(\sigma(z))\, m_p \, d\Omega = \frac{\iiint_{\Omega_p} g(\sigma(z))d\Omega}{\iiint_{\Omega_p} d\Omega} \qquad [4.16]$$

where σ denotes the stress tensor, Ω_p is an open set, and m_p is a characteristic function that is constant on Ω_p, zero outside of Ω_p, and

whose integral is 1. Here, g is assumed to be continuously differentiable with respect to its arguments. Note that $g(\sigma(z))$ might involve principal stresses, von Mises failure criterion, or some other material failure criteria. Taking the first variation of Eq. 4.16, using Eq. 3.10 [10],

$$\psi_2' = [\iiint_{\Omega_p}(g' + \nabla g^T V + g \text{ div } V)d\Omega \iiint_{\Omega_p} d\Omega$$

$$- \iiint_{\Omega_p} g \, d\Omega \iiint_{\Omega_p} \text{div } V d\Omega]/(\iiint_{\Omega_p} d\Omega)^2$$

$$= \iiint_{\Omega} \sum_{i,j=1}^{3} g_{\sigma^{ij}}(z)[\sigma^{ij}(\dot{z}) - \sigma^{ij}(\nabla z^T V)]m_p d\Omega$$

$$+ \iiint_{\Omega} \sum_{k=1}^{3} [\sum_{i,j=1}^{3} g_{\sigma^{ij}}(z)\sigma_k^{ij}(z)V^k]m_p d\Omega + \iiint_{\Omega} g \text{ div } V m_p d\Omega$$

$$- \iiint_{\Omega} g \, m_p d\Omega \iiint_{\Omega} m_p \text{ div } V d\Omega \qquad [4.17]$$

It can be shown that

$$\sigma^{ij}(\nabla z^T V) = \sum_{k,\ell=1}^{3} C^{ijk\ell}(\nabla z_\ell^{k^T} V + \nabla z^{k^T} V_\ell) \qquad [4.18]$$

and

$$\sum_{k=1}^{3} \sigma_k^{ij}(z)V^k = \sum_{k,\ell=1}^{3} C^{ijk\ell}(\nabla z_\ell^{k^T} V) \qquad [4.19]$$

Using these results, Eq. 4.17 becomes

$$\psi_2' = \iiint_{\Omega}[\sum_{i,j=1}^{3} g_{\sigma^{ij}}(z)\sigma^{ij}(\dot{z})]m_p d\Omega$$

$$- \iiint_{\Omega} \sum_{i,j=1}^{3} [\sum_{k,\ell=1}^{3} g_{\sigma^{ij}}(z)C^{ijk\ell}(\nabla z^{k^T} V_\ell)]m_p d\Omega$$

$$+ \iiint_{\Omega} g \text{ div } V m_p d\Omega - \iiint_{\Omega} g m_p d\Omega \iiint_{\Omega} m_p \text{ div } V d\Omega \qquad [4.20]$$

As in the displacement functional case, an adjoint equation is introduced by replacing $\dot{z} \in Z$ in the term on the right of Eq. 4.20 by a virtual displacement $\bar{\lambda} \in Z$ and equate the result to the energy bilinear form,

$$a_{u,\Omega}(\lambda,\bar{\lambda}) = \iint_{\Omega} \Big[\sum_{i,j=1}^{3} g_{\sigma^{ij}}(z)\sigma^{ij}(\bar{\lambda}) \Big] m_p d\Omega, \qquad \text{for all } \bar{\lambda} \in Z \qquad [4.21]$$

Denote the solution of Eq. 4.21 as $\lambda^{(2)}$. By the same method used for the displacement functional, the sensitivity formula is obtained as

$$\begin{aligned}\psi_2' = {} & \ell'_{u,V}(\lambda^{(2)}), - a'_{u,V}(z,\lambda^{(2)}) \\ & - \iiint_{\Omega} \sum_{i,j=1}^{3} \Big[\sum_{k,\ell=1}^{3} g_{\sigma^{ij}}(z) C^{ijk\ell} (\nabla z^k)^T V_\ell \Big] m_p d\Omega \\ & + \iiint_{\Omega} g \operatorname{div} V m_p d\Omega - \iiint_{\Omega} g m_p d\Omega \iiint_{\Omega} m_p \operatorname{div} V d\Omega \end{aligned} \qquad [4.22]$$

where explicit expressions of the first two terms in Eq. 4.22 for the three dimensional elastic solid can be obtained using Eq. 2.6, 2.7, 4.6, and 4.7. These explicit expressions will be derived in Section 5. Note that these terms have the same form as those of Eq. 4.15 for the three dimensional elastic solid. The difference is that terms in Eq. 4.15 are evaluated at $\lambda^{(1)}$ and terms in Eq. 4.22 are evaluated at $\lambda^{(2)}$. That is, once the expressions for terms in Eq. 4.15 are derived, they can be used for different functionals.

Finally consider a locally averaged stress functional over a test area Ω_p in a plate/plane elastic solid component,

$$\psi_3 = \iint_{\Omega} [g^1(t,w_{ij}) + g^2(\sigma(v))] m_p \, d\Omega \qquad [4.23]$$

where $g^1(t,w_{ij})$ and $g^2(\sigma(v))$ are principal stress, von Mises yield stress, or some other stress measures due to lateral displacement w and in-plane displacement field v, respectively. Here, $g^1(t,w_{ij})$ is measured at the extreme fiber and m_p is a characteristic function on that is constant on Ω_p, zero outside Ω_p, and whose integral is 1. Taking the first variation of Eq. 4.23, using Eq. 3.10,

$$\begin{aligned}\psi_3' = {} & \iint_{\Omega} \sum_{i,j=1}^{2} g^1_{w_{ij}} [\dot{w}_{ij} - (\nabla w^T V)_{ij}] \, m_p d\Omega \\ & + \iint_{\Omega} \Big[\sum_{i,j=1}^{2} g^2_{\sigma^{ij}} \sigma^{ij}(\dot{v}) \Big] m_p d\Omega + \iint_{\Omega} \operatorname{div}(g^1 V) \, m_p d\Omega \end{aligned}$$

$$- \iint_{\Omega} \sum_{i,j=1}^{2} \left[\sum_{k,\ell=1}^{2} g^2_{\sigma_{ij}}(v) C^{ijk\ell} (\nabla v^k {}^T V_\ell) \right] m_p d\Omega$$

$$+ \iint_{\Omega} g^2 \text{div } V \, m_p d\Omega - \iint_{\Omega} (g^1 + g^2) \, m_p d\Omega \iint_{\Omega} m_p \text{div } V \, d\Omega \qquad [4.24]$$

Define an adjoint equation by replacing $\dot{w}$ and $\dot{v}$ in Eq. 4.24 by virtual displacements $\bar{\eta}$ and $\bar{\xi}$, respectively, and equate terms involving $\bar{\eta}$ and $\bar{\xi}$ in Eq. 4.24 to the energy bilinear form,

$$a_{u,\Omega}(\lambda, \bar{\lambda}) = \iint_{\Omega} \left[\sum_{i,j=1}^{2} g^1_{w_{ij}} \bar{\eta}_{ij} \right] m_p d\Omega$$

$$+ \iint_{\Omega} \left[\sum_{i,j=1}^{2} g^2_{\sigma_{ij}} \sigma^{ij}(\bar{\xi}) \right] m_p d\Omega, \qquad \text{for all } \bar{\lambda} \in Z \qquad [4.25]$$

where $\lambda = [\eta, \xi^1, \xi^2]^T$ is an adjoint variable. Denote the solution of Eq. 4.25 as $\lambda^{(3)}$. By the same method used for the displacement functional, the sensitivity formula is obtained as

$$\psi'_3 = \ell'_{u,V}(\lambda^{(3)}) - a'_{u,V}(z, \lambda^{(3)}) - \iint_{\Omega} \left[\sum_{i,j=1}^{2} g^1_{w_{ij}} (\nabla w^T V) \right] m_p d\Omega$$

$$+ \iint_{\Omega} \text{div}(g^1 V) m_p d\Omega - \iint_{\Omega} \sum_{i,j=1}^{2} \left[\sum_{k,\ell=1}^{2} g^2_{\sigma_{ij}}(v) C^{ijk\ell} (\nabla v^k {}^T V_\ell) \right] m_p d\Omega$$

$$+ \iint_{\Omega} g^2 \text{div } V \, m_p d\Omega - \iint_{\Omega} (g^1 + g^2) m_p d\Omega \iint_{\Omega} m_p \text{div } V \, d\Omega \qquad [4.26]$$

where explicit expressions of the first two terms in Eq. 4.26 for the plate/plane elastic solid component can be obtained using Eqs. 2.10, 2.11, 4.6 and 4.7. These explicit expressions will be derived in Section 5. As in the displacement functional case, evaluation of the design sensitivity formula of Eq. 4.26 requires solutions z and $\lambda^{(3)}$ of Eqs. 4.1 and 4.25. Design sensitivity information for locally averaged stress functional over a test length Ω_p in a beam/truss component can be derived using the same procedure.

5. SHAPE DESIGN SENSITIVITY ANALYSIS OF STRUCTURAL COMPONENTS

In this section, explicit expressions for terms in Eqs. 4.6 and 4.7 are derived for each structural components by identifying bilinear mapping $c(\cdot,\cdot)$ and loading terms. The result is standard expressions that can be used for design sensitivity analysis of different functionals. These results can also be used for design sensitivity analysis of built-up structures which will be shown in Section 9.

A. BEAM/TRUSS

Using energy bilinear and load linear forms of Eqs. 2.1 and 2.2 for beam/truss component, Eqs. 4.6 and 4.7 become

$$\begin{aligned} a'_{u,V}(z,\bar{z}) = &\int_0^{\ell} \{-EI^1[3w^1_{xx}\bar{w}^1_{xx}V_x + (w^1_{xx}\bar{w}^1_x + w^1_x\bar{w}^1_{xx})V_{xx}] \\ &+ EI^1_x w^1_{xx}\bar{w}^1_{xx}V\}\,dx + \int_0^{\ell} \{-EI^2[3w^2_{xx}\bar{w}^2_{xx}V_x \\ &+ (w^2_{xx}\bar{w}^2_x + w^2_x\bar{w}^2_{xx})V_{xx}] + EI^2_x w^2_{xx}\bar{w}^2_{xx}V\}\,dx \\ &+ \int_0^{\ell} (-GJ\theta_x\bar{\theta}_xV_x + GJ_x\theta_x\bar{\theta}_xV)\,dx \\ &+ \int_0^{\ell} (-hEv_x\bar{v}_xV_x + h_xEv_x\bar{v}_xV)\,dx \end{aligned} \qquad [5.1]$$

and

$$\begin{aligned} \ell'_{u,V}(\bar{z}) = &\int_0^{\ell} (q^1_x\bar{w}^1V + q^1\bar{w}^1V_x)\,dx + \int_0^{\ell} (q^2_x\bar{w}^2V + q^2\bar{w}^2V_x)\,dx \\ &+ \int_0^{\ell} (r_x\bar{\theta}V + r\bar{\theta}V_x)\,dx + \int_0^{\ell} (f_x\bar{v}V + f\bar{v}V_x)\,dx \end{aligned} \qquad [5.2]$$

B. THREE DIMENSIONAL ELASTIC SOLID

Using energy bilinear and load linear forms of Eqs. 2.6 and 2.7 for three dimensional elastic solid, Eqs. 4.6 and 4.7 become

$$a'_{u,V}(z,\bar{z}) = -\iiint_\Omega \sum_{i,j=1}^{3} [\sigma^{ij}(z)\varepsilon^{ij}(\nabla\bar{z}^T V) + \sigma^{ij}(\bar{z})\varepsilon^{ij}(\nabla z^T V)]d\Omega$$
$$+ \iiint_\Omega \nabla[\sum_{i,j=1}^{3} \sigma^{ij}(z)\varepsilon^{ij}(\bar{z})]^T V d\Omega + \iiint_\Omega [\sum_{i,j=1}^{3} \sigma^{ij}(z)\varepsilon^{ij}(\bar{z})]\text{div } V d\Omega \quad [5.3]$$

and

$$\ell'_{u,V}(\bar{z}) = \iiint_\Omega \sum_{i=1}^{3} \bar{z}^i(\nabla f^{i^T} V)d\Omega + \iiint_\Omega [\sum_{i=1}^{3} f^i\bar{z}^i] \text{ div } V d\Omega$$
$$+ \iint_{\Gamma_2} \{-\sum_{i=1}^{3} T^i(\nabla\bar{z}^{i^T} V) + (\nabla[\sum_{i=1}^{3} T^i\bar{z}^i]^T n + H[\sum_{i=1}^{3} T^i\bar{z}^i])(V^T n)\}d\Gamma \quad [5.4]$$

It can be verified that

$$\sum_{i,j=1}^{3} \sigma^{ij}(z)\varepsilon^{ij}(\nabla\bar{z}^T V) = \sum_{i,j=1}^{3} \sigma^{ij}(z)(\nabla\bar{z}^i_j{}^T V + \nabla\bar{z}^{i^T} V_j) \quad [5.5]$$

and

$$\nabla[\sum_{i,j=1}^{3} \sigma^{ij}(z)\varepsilon^{ij}(\bar{z})]^T V = \sum_{i,j=1}^{3} [\sigma^{ij}(z)(\nabla\bar{z}^i_j{}^T V) + \sigma^{ij}(\bar{z})(\nabla z^i_j{}^T V)] \quad [5.6]$$

where $V_j = [V^1_j, V^2_j, V^3_j]^T$. Using the above results, Eqs. 5.3 becomes

$$a'_{u,V}(z,\bar{z}) = -\iiint_\Omega \sum_{i,j=1}^{3} [\sigma^{ij}(z)(\nabla\bar{z}^{i^T} V_j) + \sigma^{ij}(\bar{z})(\nabla z^{i^T} V_j)]d\Omega$$
$$+ \iiint_\Omega [\sum_{i,j=1}^{3} \sigma^{ij}(z)\varepsilon^{ij}(\bar{z})] \text{ div } V d\Omega \quad [5.7]$$

C. PLATE/PLANE ELASTIC SOLID

As in the beam/truss and three dimensional elastic solid components, explicit expressions for terms in Eqs. 4.6 and 4.7 can be obtained using energy bilinear and load linear forms of Eqs. 2.10 and 2.11 for plate/plane elastic solid component. For plane elastic solid component, Eqs. 5.7 and 5.4 remain valid, with limits of summation running from 1 to 2 and an appropriate modification of the generalized Hooke's Law of Eq. 2.5. Equations 4.6 and 4.7 become, for plate/plane elastic solid component,

$$
\begin{aligned}
a'_{u,V}(z,\bar{z}) = \iint_{\Omega} & -\hat{D}(t)\{4(w_{11}\bar{w}_{11}V_1^1 + w_{22}\bar{w}_{22}V_2^2) + [\nu(w_{11}\bar{w}_{22} + w_{22}\bar{w}_{11}) \\
& - (w_{11}\bar{w}_{11} + w_{22}\bar{w}_{22}) + 2(1-\nu)w_{12}\bar{w}_{12}]\operatorname{div} V \\
& + 2(w_{11}\bar{w}_{12} + w_{12}\bar{w}_{11} + w_{22}\bar{w}_{12} + w_{12}\bar{w}_{22})(V_2^1 + V_1^2) \\
& + [w_1\bar{w}_{11} + w_{11}\bar{w}_1 + \nu(w_1\bar{w}_{22} + w_{22}\bar{w}_1)]V_{11}^1 \\
& + [w_1\bar{w}_{22} + w_{22}\bar{w}_1 + \nu(w_1\bar{w}_{11} + w_{11}\bar{w}_1)]V_{22}^1 \\
& + [w_2\bar{w}_{11} + w_{11}\bar{w}_2 + \nu(w_2\bar{w}_{22} + w_{22}\bar{w}_2)]V_{11}^2 \\
& + [w_2\bar{w}_{22} + w_{22}\bar{w}_2 + \nu(w_2\bar{w}_{11} + w_{11}\bar{w}_2)]V_{22}^2 \\
& + 2(1-\nu)[(w_1\bar{w}_{12} + w_{12}\bar{w}_1)V_{12}^1 + (w_2\bar{w}_{12} + w_{12}\bar{w}_2)V_{12}^2]\} \\
& + \frac{Et^2}{4(1-\nu^2)}[w_{11}\bar{w}_{11} + \nu(w_{11}\bar{w}_{22} + w_{22}\bar{w}_{11}) + w_{22}\bar{w}_{22} \\
& + 2(1-\nu)w_{12}\bar{w}_{12}]\nabla t^T V \, d\Omega \\
& + \iint_{\Omega}\{-t\sum_{i,j=1}^{2}[\sigma^{ij}(v)(\overline{\nabla v}^{i\,T}V_j) + \sigma^{ij}(\bar{v})(\nabla v^{i\,T}V_j) \\
& - \sigma^{ij}(v)\varepsilon^{ij}(\bar{v})\operatorname{div} V] + \sum_{i,j=1}^{2}\sigma^{ij}(v)\varepsilon^{ij}(\bar{v})\nabla t^T V\}d\Omega
\end{aligned}
\qquad [5.8]
$$

and

$$
\begin{aligned}
\ell'_{u,V}(\bar{z}) = & \iint_{\Omega}[\bar{w}(\nabla q^T V) + q\bar{w}\operatorname{div} V]d\Omega \\
& + \iint_{\Omega}\sum_{i=1}^{2}[\bar{v}^i(\nabla f^{i\,T}V) + f^i\bar{v}^i\operatorname{div} V]d\Omega \\
& + \int_{\Gamma}\sum_{i=1}^{2}\{-T^i(\overline{\nabla v}^{i\,T}V) + [\nabla(T^i\bar{v}^i)^T n + HT^i\bar{v}^i](V^T n)\}d\Gamma \\
& + \sum_{i=1}^{2}[T^i\bar{v}^i V_T\big|_{p_2} - T^i\bar{v}^i V_T\big|_{p_1}]
\end{aligned}
\qquad [5.9]
$$

In Eq. 5.9, H is the curvature of the loaded boundary Γ^2 and the last two terms on the right account for corner effects due to movement of points p_1

and p_2 in Fig. 2.5 [21]. In these two terms, the notation $\Big|_{p_i}$ indicates that the terms are evaluated at point p_i and V_T is the component of velocity V tangent to Γ, which is positive if it is in a counter-clockwise direction in Fig. 2.5.

Results given in Eqs. 5.1, 5.2, 5.4, and 5.7 - 5.9 can be used in Eqs. 4.15, 4.22, and 4.26 for each structural component and each functional. This allows one to develop a modular computer program that will carry out numerical integrations of terms in Eqs. 5.1, 5.2, 5.4, and 5.7 - 5.9 using the same shape functions that are employed in finite element analysis codes. The result will then be a general algorithm and numerical method for design sensitivity analysis that can be implemented with existing finite element codes which will be discussed in Section 6.

6. IMPLEMENTATION OF DESIGN SENSITIVITY ANALYSIS WITH EXISTING FINITE ELEMENT CODES

To obtain design sensitivity information, Eqs. 4.1 and 4.11 must be solved for displacement functionals and Eqs. 4.1, 4.21 and 4.25 must be solved for stress functionals. Once the original and adjoint structures are solved, one can integrate Eqs. 4.15, 4.22, and 4.26 numerically to obtain the desired sensitivity information. The finite element method can be viewed as an application of the Galerkin method to Eqs. 4.1, 4.11, 4.21, and 4.25 for an approximate solution of the boundary-value problem. Note that the energy bilinear forms for Eqs. 4.1, 4.11, 4.21, and 4.25 are same. Hence, the adjoint structures of Eqs. 4.11, 4.21, and 4.25 are the same as that of Eq. 4.1, with different adjoint loads. The adjoint load of Eq. 4.11, is a simple unit load at the point $\hat{x}$ in the positive direction of $z(\hat{x})$. To calculate the adjoint load using the load functional on the right side of Eqs. 4.21 and 4.25, one should use the same shape functions that are used in the finite element code. Since m_p is a characteristic function defined on finite element Ω_p, numerical integration of the load functional is done on Ω_p only and the adjoint equivalent nodal force acts only on the nodal points of Ω_p.

For numerical implementation with existing finite element codes, one can proceed as in the flow chart of Fig. 6.1. In the beginning, the model is defined by identifying the finite element model, original structural load, design variables, and constraint functionals. In the next step, an

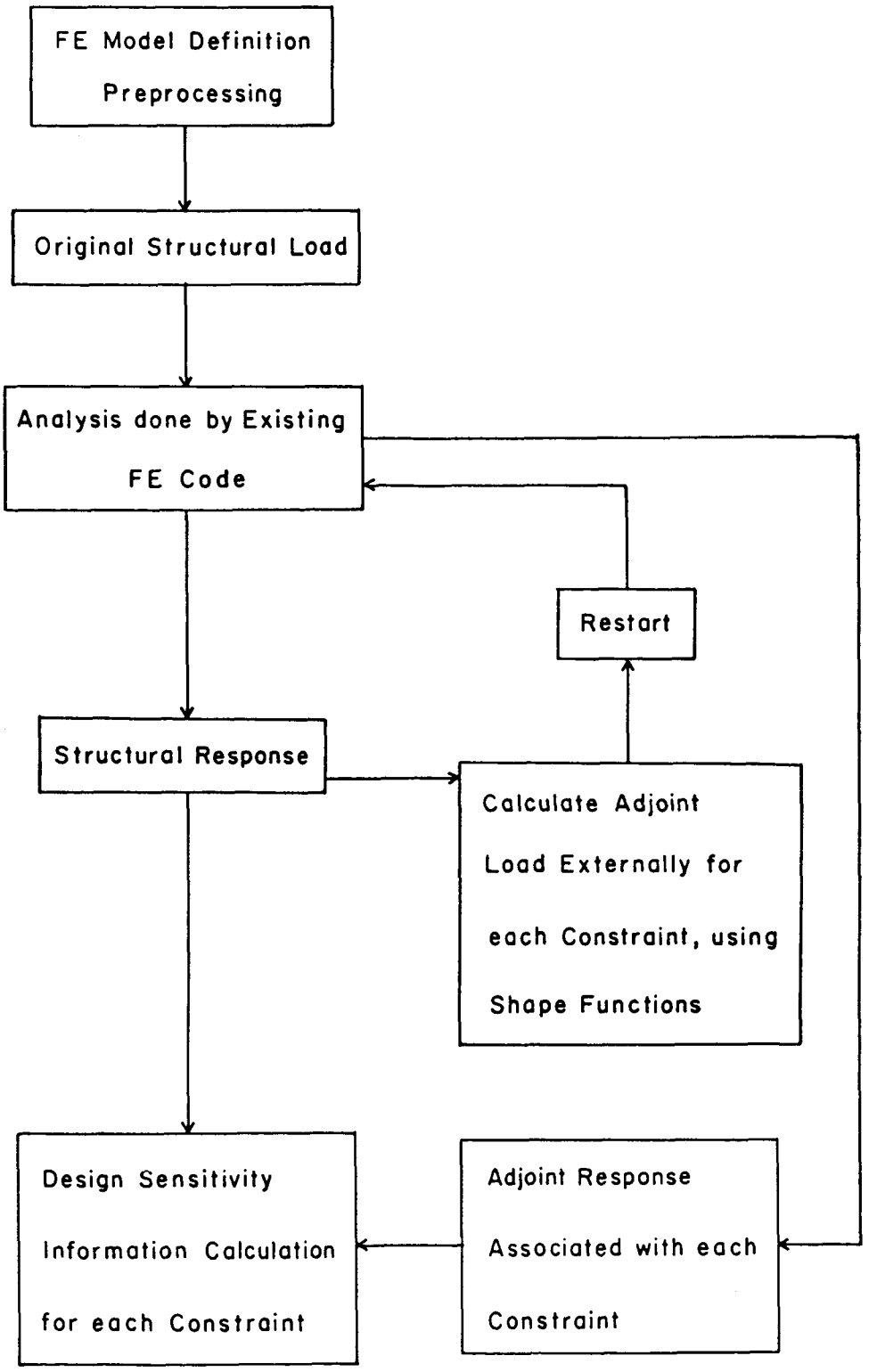

Figure 6.1 Flowchart of Design Sensitivity Calculation Procedure

existing finite element code is called to obtain structural response. With the structural response obtained, one calculates an adjoint load, external to the finite element code, using the shape functions of the code. The adjoint load is then input to the finite element code, to obtain an adjoint response for each constraint functional. For adjoint analysis, one can use the multiloading (restart) option of the finite element code, so that only forward and backward substitutions are performed to obtain each adjoint response. Using the original and adjoint structural responses, design sensitivity information is calculated for each constraint functional, by carrying out only numerical integration. This procedure allows one to carry out calculations outside finite element codes, using postprocessing data only. That is, the design sensitivity software does not have to be imbedded into finite element codes. Moreover, the method does not require differentiation of stiffness and mass matrices and the uncertainty of numerical accuracy associated with selection of a finite difference perturbation can be eliminated.

7. NUMERICAL EXAMPLES

Substantial numerical experimentation has been carried out using the material derivative shape design sensitivity analysis formulation, with the boundary method. Good results have been reported [2,23] for a variety of single structural components. These studies have shown that great care must be taken in projecting stress information to the boundary to achieve acceptable design sensitivity accuracy. Higher order elements and extrapolation from Gauss points have been shown to be essential in achieving acceptable accuracy. Substantially inaccurate results have been observed when low order elements are used and elementary boundary projection approaches are employed.

Numerical experimentation with the domain method [15,16,18,22] has indicated consistently good results for structural components, without the requirement for sophisticated elements, clever boundary projection methods, or drastically refined grids. In order to be more quantitative, two examples are discussed to permit numerical comparison.

Consider a plane elastic solid that is composed of two materials of substantially different modulus of elasticity ($E^2/E^1 = 7.65$) and subjected to simple tension, as shown in Fig. 7.1. The finite element configuration,

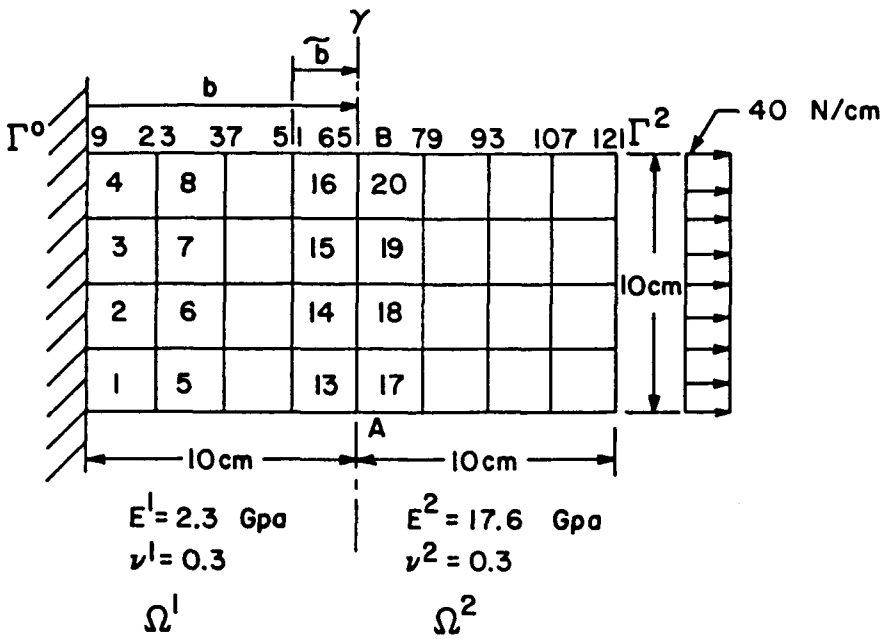

Figure 7.1 Interface Problem

dimensions, material properties of each body, and loading conditions are shown in Fig. 7.1. Body i occupies domain Ω^i, i=1,2, AB is the interface boundary γ, and Γ^0 and Γ^2 are the clamped and loaded boundaries, respectively. The design variable b controls the position of the interface boundary γ, while the overall dimensions of the structure are fixed.

The expression for design sensitivity of the von Mises yield stress functional associated with interface boundary movement with the domain method is obtained by simply adding results of Eq. 4.26 for both segments of the structure. For the plane stress interface problem, terms in Eq. 4.26 due to plate bending must be dropped. For the boundary method, design sensitivity computations are carried out in Ref. 10 (Eq. 42) that is analytically equivalent to the result of the domain method.

For numerical computation, the finite element method is used to approximate the state and adjoint equations of Eqs. 4.1 and 4.25, respectively. In order to compute the design sensitivity expressions of Eq. 4.26 one must define a design velocity field V that satisfies regularity properties defined in Refs. 2 and 9, in terms of variations in the design variable b. To have a continuous design velocity field, one may define

$$\left.\begin{aligned} V^1 &= \frac{x_1}{b}\,\delta b \\ V^2 &= 0 \end{aligned}\right\}, \text{ on } \Omega^1 \qquad [7.1]$$

and

$$\left.\begin{aligned} V^1 &= \frac{20 - x_1}{20 - b} \\ V^2 &= 0 \end{aligned}\right\}, \text{ on } \Omega^2 \qquad [7.2]$$

The finite element model shown in Fig. 7.1 contains 32 elements, 121 nodal points, and 224 degrees-of-freedom. The 8-noded isoparametric element is employed for design sensitivity analysis. For the boundary method, stresses and strains are obtained at Gauss points and extrapolated to the boundary to obtain accurate results on the boundary [23]. Define ψ^1 and ψ^2 as the functional values for the initial design b and modified design b + δb, respectively. Let $\Delta\psi = \psi^2 - \psi^1$ and let ψ' be the predicted difference from sensitivity analysis. The ratio $\psi'/\Delta\psi$ times 100 is used as a measure of accuracy; i.e., 100% means that the predicted change is exactly the same as the actual change. Notice that this accuracy measure will not give meaningful information when $\Delta\psi$ is very small compared to ψ^1, because the difference $\Delta\psi$ may lose precision due to the subtraction $\psi^2 - \psi^1$.

Numerical results with a 3% design change; i.e., $\delta b = 0.03b$, are shown in Table 7.1 for the boundary method and in Table 7.2 for the domain method. Due to symmetry, sensitivity results for only the lower half of the structure are given. These results indicate that the domain method gives excellent results, whereas accuracy of the boundary method is not acceptable. For elements 22 and 29, the predicted values are less accurate than others. However, the magnitude of actual differences $\Delta\psi$ for those elements are smaller than others, so $\Delta\psi$ may lose precision.

A disadvantage of the domain method is that a velocity field must be defined in the domain and satisfy regularity properties. There is no unique way of defining domain velocity fields for a given normal velocity field ($V^T n$) on the boundary. Also, numerical evaluation of the sensitivity result of Eq. 4.26 is more complicated than evaluation of Eq. 42 of Ref. 10, since Eq. 4.26 requires integration over the entire domain, whereas Eq. 42 of Ref. 10 requires integration over only the variable boundary. This problem can be alleviated by introducing a boundary layer [16] of finite elements that vary during the perturbation of the shape of

Table 7.1. Boundary Method for Interface Problem

El. No.	ψ^1	ψ^2	$\Delta\psi$	ψ'	$(\psi'/\Delta\psi x100)\%$
1	393.01304	393.17922	0.16618	0.20403	122.8
2	364.37867	364.76664	0.38796	0.67218	173.3
5	388.07514	388.36215	0.28701	0.56684	197.5
6	402.26903	402.83406	0.56503	0.42080	74.5
9	386.43461	386.84976	0.41515	-0.08520	-20.5
10	407.14612	407.48249	0.33637	0.14159	42.1
13	388.59634	388.95414	0.35780	-0.53089	-148.4
14	379.04276	379.25247	0.20971	-1.90134	-906.6
17	441.68524	442.25032	0.56507	-13.85905	-2452.6
18	424.05820	425.22910	1.17089	-13.63066	-1164.1
21	424.19015	424.70840	0.51825	-0.21408	-41.3
22	378.85433	378.97497	0.12064	0.76770	636.4
25	407.71528	408.23368	0.51840	0.49780	96.2
26	387.87307	387.32342	-0.54962	-0.48837	88.9
29	400.61014	400.60112	-0.00903	0.01423	-157.7
30	394.61705	394.00702	-0.61003	-0.57794	94.7

Table 7.2. Domain Method for Interface Problem

El. No.	ψ^1	ψ^2	$\Delta\psi$	ψ'	$(\psi'/\Delta\psi x100)\%$
1	393.01304	393.17922	0.16618	0.17954	108.0
2	364.37867	364.76664	0.38796	0.37840	97.5
5	388.07514	388.36215	0.28701	0.28671	99.9
6	402.26903	402.83406	0.56503	0.59634	105.5
9	386.43461	386.84976	0.41515	0.41515	100.6
10	407.14612	407.48249	0.33637	0.33637	109.6
13	388.59634	388.95414	0.35780	0.37548	104.9
14	379.04276	379.25247	0.20971	0.20159	96.1
17	441.68524	442.25032	0.56507	0.57069	101.0
18	424.05820	425.22910	1.17089	1.12871	96.4
21	424.19015	424.70840	0.51825	0.53919	104.0
22	378.85433	378.97497	0.12064	0.06396	53.0
25	407.71528	408.23368	0.51840	0.51710	99.7
26	387.87307	387.32342	-0.54962	-0.56083	102.0
29	400.61014	400.60112	-0.00903	-0.00298	33.0
30	394.61705	394.00702	-0.61003	-0.58529	95.9

a structural component. This approach is illustrated schematically in Fig. 7.2. The domain Ω is divided into subdomains Ω_1 and Ω_2, with inner

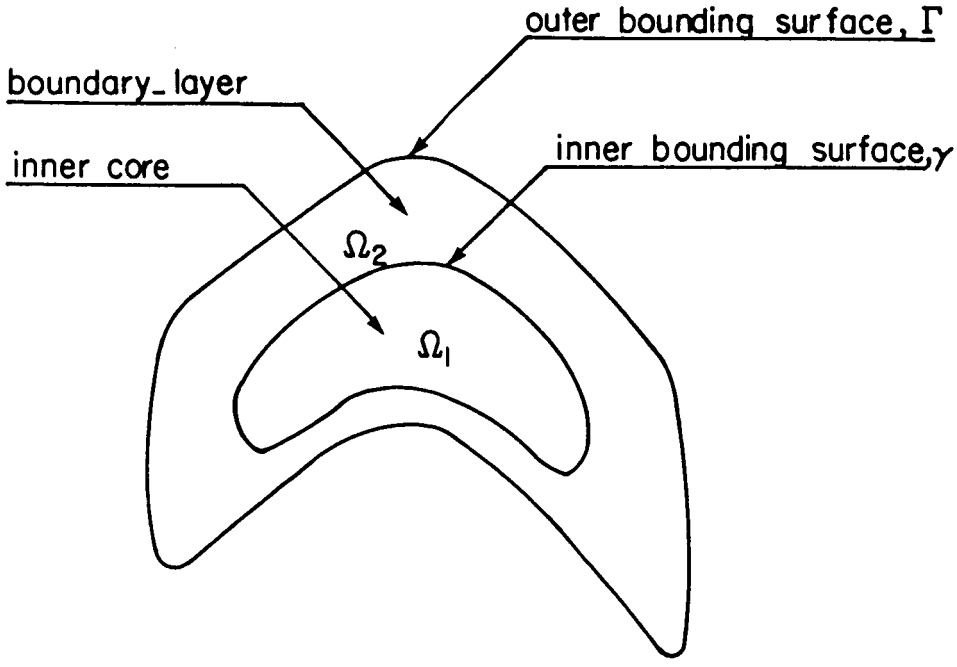

Figure 7.2 Boundary Layer

core Ω_1 held fixed and only boundary layer Ω_2 modified. In this way, the velocity field need be defined only on Ω_2. The thickness of the boundary layer Ω_2 will depend on trade-offs between numerical accuracy and numerical efficiency. In practice, Ω_1 can be a substructure of the finite element model.

To demonstrate feasibility of the boundary layer approach, two examples are solved by the boundary layer approach. The first example is the plane stress interface problem discussed in this section. For a body of given geometry there is a large number of possible boundary-layers, some of which are better than others, from the viewpoint of accuracy and efficiency. It is difficult to estimate the size and location of the best boundary-layers in advance. They can be determined by analyzing the structure and measuring the strain energy density [24].

The boundary-layer is chosen to include elements 13 thru 20 in Fig. 7.1. The design variable $\tilde{b}$ for this case is distance between node 51 and node 65 in Fig. 7.1. Consequently, regions outside the boundary-layer remain unchanged. Numerical results with a 3% design change are shown in Table 7.3 for the boundary-layer approach. Due to symmetry, the shape design sensitivity analysis results of the lower half of the structure are shown. Shape design sensitivity analysis results obtained with the boundary-layer approach are excellent, as shown in Table 7.3.

Table 7.3. Boundary Layer Approach for Interface Problem ($E^2/E^1 = 7.65$)

El. No.	ψ^1	ψ^2	$\Delta\psi$	ψ'	$(\psi'/\Delta\psi \times 100)\%$
1	393.01304	393.07967	0.06663	0.06770	101.6
2	364.37867	364.29542	-0.08325	-0.08412	101.0
5	388.07514	388.20344	0.12830	0.12916	100.7
6	402.26903	402.19633	0.07270	-0.07126	98.0
9	386.43461	386.47687	0.04227	0.04103	97.1
10	407.14612	407.46571	0.31960	0.32954	103.1
13	388.59634	388.70300	0.10666	0.10834	101.6
14	379.04276	379.52487	0.48210	0.48590	100.8
17	441.68524	442.17008	0.48484	0.47615	98.2
18	424.05820	425.31717	1.25897	1.23636	98.2
21	424.19015	424.44270	0.25254	0.25680	101.7
22	378.85433	378.99459	0.14025	0.11902	84.9
25	407.71528	407.99105	0.27577	0.27248	98.8
26	387.87304	387.59778	-0.27526	-0.27540	100.0
29	400.61014	400.62571	0.01557	0.01543	99.1
30	394.61705	394.45461	-0.16244	-0.16104	99.1

Next, to test validity of the boundary-layer approach, Young's modulus is changed to $E^1 = 0.2$ MPa and $E^2 = 100$ MPa for Ω^1 and Ω^2, respectively. In other words, the ratio between E^2 and E^1 is raised to 500, from 7.65, to check a more severe condition. Design sensitivity results are given in Table 7.4. Accuracy of design sensitivity is excellent. For elements 9 and 22, the magnitude of actual change are small, so finite differences may not be accurate. Numerical results obtained with the boundary method given in Ref. 16, indicates that worse results arise if the ratio E^2/E^1 is increased.

Results for the plane stress interface problem clearly indicate that the boundary approach may have considerable difficulty in handling problems with singular characteristics. Accuracy of the boundary approach rapidly deteriorates in the vicinity of a singularity. On the other hand, the boundary-layer approach can give good sensitivity results throughout the domain. Also, in this interface problem, 56% of cpu time is saved by using the boundary-layer approach instead of the domain approach, without sacrificing accuracy of design sensitivity.

Next, the classical fillet shown in Fig. 7.3 is used to study accuracy of the boundary layer approach. The design for this problem is the shape

Table 7.4. Boundary Layer Approach for Interface Problem ($E^2/E^1 = 500$)

El. No.	ψ^1	ψ^2	$\Delta\psi$	ψ'	$(\psi'/\Delta\psi \times 100)\%$
1	392.30557	392.39359	0.08802	0.08926	101.4
2	365.24352	365.14384	-0.09967	-0.10047	100.8
5	386.63113	386.77199	0.14086	0.14138	100.4
6	402.93637	402.89886	-0.03752	-0.03477	92.7
9	386.58037	386.56330	-0.01706	-0.02016	118.2
10	403.05338	403.58214	0.52876	0.54150	102.4
13	392.16507	392.15462	-0.01046	-0.01033	98.8
14	365.55409	366.17638	0.62229	0.62552	100.5
17	477.04122	478.18542	1.14420	1.11943	97.8
18	440.11698	442.56025	2.44327	2.39258	97.9
21	442.63898	443.09215	0.45317	0.46452	102.5
22	362.56664	362.67559	0.10895	0.07117	65.3
25	412.83466	413.32142	0.48676	0.48000	98.6
26	379.90505	379.41355	-0.49149	-0.49033	99.8
29	401.08818	401.11877	0.03059	0.03031	99.1
30	391.19616	390.92213	-0.27403	-0.27158	99.1

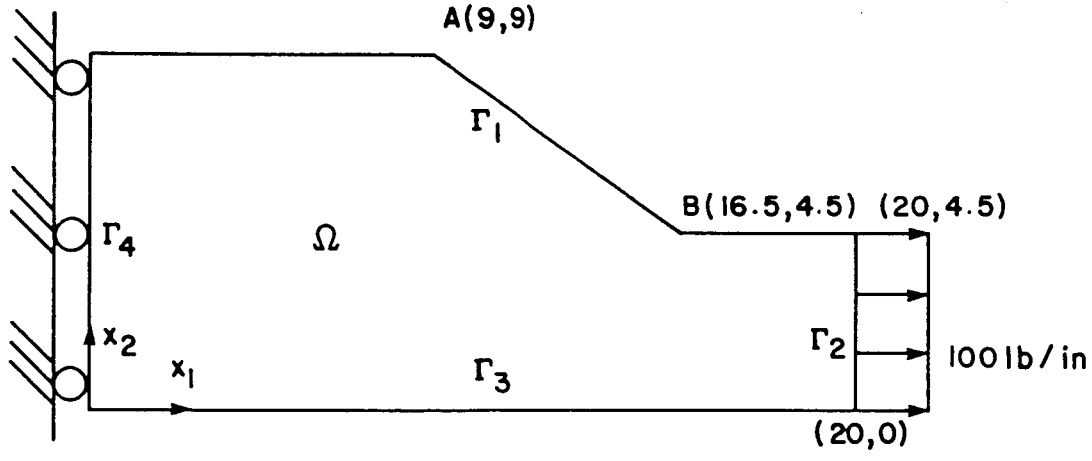

Figure 7.3 Fillet

of the varying boundary Γ_1 between points A and B, without moving these two points. B-spline representation is used for the varying boundary Γ_1. Due to symmetry, only the upper half of a fillet is analyzed. Dimensions of the structure and applied loads are given in Fig. 7.3. For material property, Young's modulus and Poisson's ratio are 3.0×10^7 psi and $\nu = 0.293$, respectively. The segment Γ_3 is the center-line of the fillet

and Γ_2 is the uniformly loaded edge. Sensitivity of von Mises stress averaged over individual finite elements is employed to test accuracy of the boundary-layer approach. The expression for design sensitivity is obtained from Eq. 4.26 with nonzero velocity field on the boundary layer.

The boundary-layer (27% of the total area) shown in Fig. 7.4 is chosen after analyzing the structure and measuring the strain energy density. In Fig. 7.5, a finite element model with optimized boundary profile Γ_1 and 319 elements and 1994 active degrees-of-freedom is shown. The element type used is an 8-node isoparametric element.

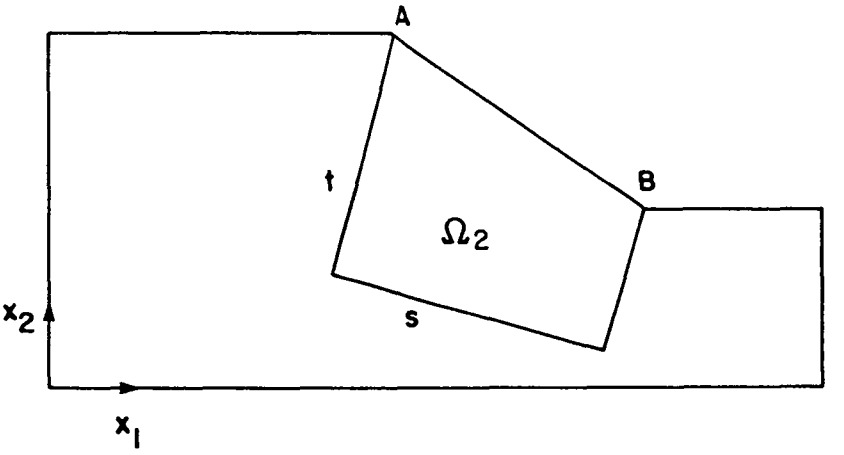

Figure 7.4 Boundary-Layer of Fillet

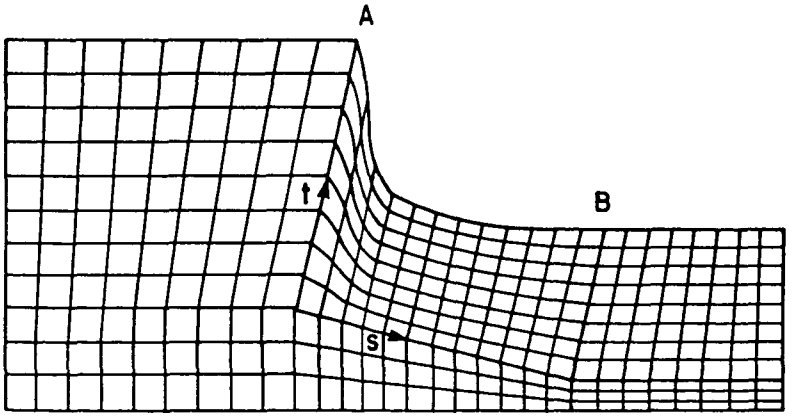

Figure 7.5 Finite Element Mesh of Fillet

In Table 7.5, shape design sensitivity results for a fillet with optimized boundary profile Γ_1 (see Fig. 7.5) are given, obtained with 0.1% design perturbation. From Table 7.5, it can be seen that this approach can yield excellent shape design sensitivity results.

Table 7.5. Boundary Layer Approach for Fillet

El. No.	ψ^1	ψ^2	$\Delta\psi$	ψ'	$(\psi'/\Delta\psi \times 100)\%$
3	306.91341	307.18632	0.27291	0.27802	101.9
13	326.43889	326.65762	0.21873	0.22298	101.9
23	386.17664	386.33965	0.16301	0.16693	102.4
33	471.26543	471.38415	0.11872	0.12219	102.9
43	570.91518	570.95727	0.04209	0.04294	102.0
53	669.26309	669.16035	-0.10274	-0.10693	104.1
63	736.39264	736.12922	-0.26341	-0.27187	103.2
73	682.49507	682.26122	-0.23385	-0.23826	101.9
83	761.77304	761.44391	-0.32913	-0.33921	103.1
93	911.47561	911.14248	-0.33314	-0.33869	101.7
103	764.32105	764.00138	-0.31967	-0.32424	101.4
113	884.95173	884.66270	-0.28902	-0.28788	99.6
123	768.06301	767.74016	-0.32285	-0.32715	101.3
133	857.37113	857.10506	-0.26607	-0.26249	98.7
143	999.87828	999.87875	0.00047	0.00045	95.4
153	1009.58379	1009.52243	-0.06137	-0.05071	82.6
163	1000.99060	1000.92960	-0.06100	-0.05863	96.1
173	999.42406	999.33430	-0.08976	-0.08873	98.8
183	1001.15587	1001.04706	-0.10881	-0.10766	98.9
193	958.70044	958.26124	-0.43919	-0.44416	101.1
203	980.40747	980.03216	-0.37531	-0.37607	100.2
213	993.57091	993.33304	-0.23787	-0.23708	99.7
223	1000.47920	1000.29798	-0.18122	-0.17969	99.2
233	762.37599	762.01522	-0.36076	-0.40403	112.0
243	778.19389	777.74914	-0.44475	-0.45837	103.1
253	881.29226	880.57387	-0.71838	-0.69488	96.7
263	1220.22663	1219.47520	-0.75143	-0.72158	96.0
273	835.72273	835.22544	-0.49729	-0.48555	97.6
283	922.89834	922.29381	-0.60453	-0.58846	97.3
293	1033.88104	1033.07352	-0.80752	-0.77133	95.5
303	1093.40867	1090.74702	-2.66165	-2.67483	100.5
313	936.38542	936.01573	-0.36969	-0.37920	102.6

8. AUTOMATIC REGRIDDING FOR SHAPE DESIGN

For numerical implementation of shape design sensitivity analysis, one must parameterize the boundary Γ of the domain Ω. For this purpose, one may use Bezier curves or surfaces [25]. The next step is to develop a general method of defining and computing a velocity field in the domain, in terms of the perturbation of the boundary Γ. Moreover, the velocity field must satisfy certain regularity conditions. It is shown in Refs. 2 and 9 that C^1-regular and C^2-regular velocity fields are sufficient for

shape design sensitivity analysis of truss and elastic solid problems and beam and plate problems, respectively. However, observing Eqs. 5.1, 5.2, 5.4, and 5.7 - 5.9, one may relax these regularity conditions. That is, for truss and elastic solid problems, the highest order derivative of the velocity field that appears in Eqs. 5.1, 5.2, 5.4, and 5.7 - 5.9 is one. Thus, one may use a C^0-regular velocity field with an integrable first derivative. Similarly, one may use a C^1-regular velocity field with an integrable second derivative for beam and plate problems. Therefore, regularity of the velocity field must be at least at the level of regularity of the displacement field of the structural component considered. This suggests use of displacement shape functions to systematically define the velocity field in the domain. Moreover, one can select a velocity field that obeys the governing equation of the structure. That is, the perturbation of the boundary can be considered as a displacement at the boundary. With no additional external forces and a given displacement at the boundary, one can use the finite element code to find the displacement (domain velocity) field that satisfies the required regularity conditions. Thus

$$[K]\{V\} = \{f\} \qquad [8.1]$$

where $[K]$ is the reduced stiffness matrix, $\{V\}$ is the velocity vector of the nodes of varying domain, and $\{f\}$ is the unknown ficticious boundary force that produces a perturbation of the boundary. In segmented form, Eq. 8.1 becomes

$$\begin{bmatrix} K_{bb} & K_{bd}^T \\ K_{bd} & K_{dd} \end{bmatrix} \begin{Bmatrix} V_b \\ V_d \end{Bmatrix} = \begin{Bmatrix} f_b \\ 0 \end{Bmatrix} \qquad [8.2]$$

where $\{V_b\}$ is the given perturbation of nodes on the boundary, $\{V_d\}$ is the node velocity vector in the interior of the domain and $\{f_b\}$ is the ficticious boundary force acting on the varying boundary. Equation for the unknown interior node velocity vector can be obtained from Eq. 8.2 as

$$[K_{dd}]\{V_d\} = -[K_{bd}]\{V_b\} \qquad [8.3]$$

If Bezier curves or surfaces [17] are used for boundary representation, positions of control points are selected as design parameter b_i, i = 1,2,...,k. To use Eqs. 4.15, 4.22, and 4.26 for sensitivity computation, interior node velcity vector $\{V_d\}$ should be expressed in terms of variations of design parameter δb_i, i = 1,2,...,k. To obtain this expression, boundary perturbation $\{V_b\}$ should be written in terms of variation δb of the design parameter. Once the inverse matrix $[K_{dd}]^{-1}$ is obtained, Eq. 8.3 can be used to express $\{V_d\}$ in terms of the variation δb of design parameter. However, this requires large computational effort. To gain computational efficiency, following method is used: first by pertubing a design parameter b_i a unit magnitude, boundary perturbation $\{V_b\}$ can be obtained. Then Eq. 8.3 can be solved to obtain $\{V_d\}$. Using $\{V_d\}$ and displacement shape functions, Eqs. 4.15, 4.22, or 4.26 can be evaluated which gives $\frac{\partial \psi}{\partial b_i}$. This method requires to solve Eq. 8.3 k times. However, much as in the adjoint analysis, this is an efficient calculation, if Eq. 8.3 has already been solved, requiring only evaluation of the solution of the same set of finite element equations with different right side for each unit perturbation of b_i, i = 1,2,...,k. Once design change has been determined using iterative design process, regridding of interior grid points can be carried out using $\{V_d\}$ of Eq. 8.3.

The automatic regridding method presented here can be used with the boundary-layer approach very effectively. That is, for the fixed domain Ω_1, V_d can be set equal to zero and thus reduce the dimension of $[K_{dd}]$ in Eq. 8.3.

To demonstrate feasibility of the method, an engine bearing cap shown in Fig. 8.1 is treated. The engine bearing cap is modeled as a three dimensional elastic solid. Due to symmetry, only the right half of the cap is analyzed. The finite element configuration and loading conditions are shown in Fig. 8.1. The material used is steel with Young's modulus and Poisson's ratio of $E = 1.0 \times 10^7$ psi and $\nu = 0.3$, respectively. The finite element model shown in Fig. 8.1 contains 82 elements, 768 nodal points, and 2111 degrees-of-freedom. For analysis, ANSYS finite element STIF95 [26], which is a 20-noded isoparametric element, is used.

The design variables for this problem are the shape of the varying surface Γ_1, distance C_5 of clamping bolt center line AB, and distance C_6 of edge from cap centerline (Fig. 8.2). For surface Γ_1, a Bezier surface

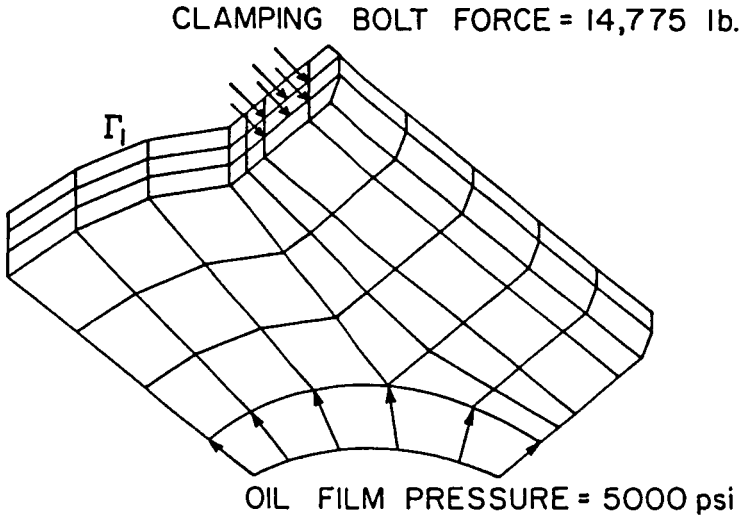

Figure 8.1 Engine Bearing Cap

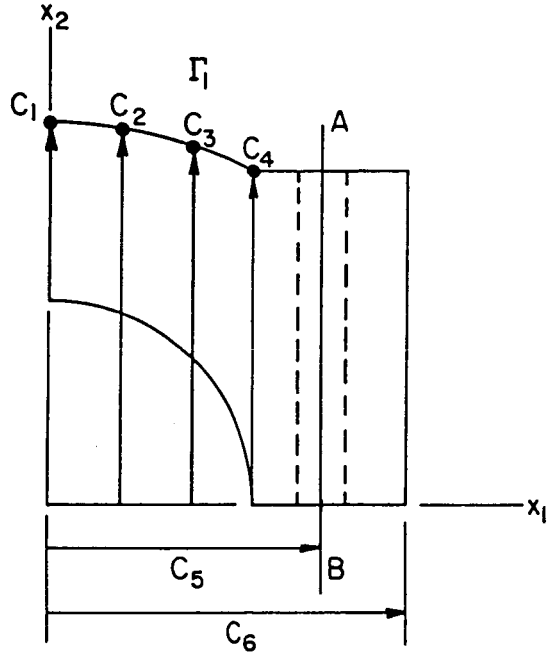

Figure 8.2 Shape Design Parameters of Engine Bearing Cap

with 4 x 4 control points is used. For simplicity, only x_2-coordinates of four control points C_1 thru C_4 are allowed to be varying. That is, surface Γ_1 has curvature in the x_1-direction only.

The expression for design sensitivity of von Mises stress averaged over individual finite element is obtained from Eq. 4.22. Numerical

computation of design sensitivity information has been carried out using ANSYS finite element code [26] and the computational procedure of Section 6. For computation of domain velocity vector, Eq. 8.2 is solved using ANSYS finite element code.

Numerical results with a 1% design change are shown in Table 8.1 for randomly selected finite elements. Accuracy of design sensitivity is excellent except for elements 5, 22, 36, 56, and 57 where the magnitudes of actual change are small.

Table 8.1. Shape Sensitivity of Engine Bearing Cap

El. No.	ψ^1	ψ^2	$\Delta\psi$	ψ'	$(\psi'/\Delta\psi \times 100)\%$
1	9829.4564	9727.3229	-102.1335	-109.7298	107.4
2	9631.2028	9565.8641	-65.3387	-70.6936	108.2
4	10620.3320	10648.0140	27.6820	25.7748	93.1
5	11444.4800	11448.0190	3.5390	0.4482	12.7
7	13584.5710	13604.0520	19.4810	17.5377	90.0
8	13641.4950	13674.1020	32.6070	31.2587	95.9
10	17933.5910	17964.5170	30.9260	29.8750	96.6
11	18498.6300	18526.7900	28.1600	27.5316	97.8
13	21202.2630	21222.8600	20.5970	20.559	100.8
14	34270.5140	34294.7650	24.2510	23.7614	98.0
16	8367.4820	8152.6800	-214.8020	-230.0584	107.1
18	9686.1116	9652.6069	-33.5047	-38.2462	114.2
20	12670.2480	12634.3500	-35.8980	-38.4216	107.0
22	16248.4050	16256.2990	7.8940	6.3254	80.1
24	30901.3690	30862.5960	-38.7730	-36.4113	93.9
26	7311.4083	6999.4094	-311.9989	-321.7022	103.1
27	6857.7422	6519.3747	-338.3675	-344.1961	101.7
29	7917.4211	7774.3107	-143.1104	-148.4639	103.7
30	7234.2502	7081.2085	-153.0417	-159.7947	104.4
32	9528.8157	9395.4689	-133.3468	-137.7809	103.3
33	8521.5076	8387.1466	-134.3610	-141.4600	105.3
35	13328.4650	13264.9790	-63.4860	-59.4243	93.6
36	12091.2310	12159.1600	67.9290	87.2240	128.4
38	24661.4990	23849.7610	-811.7380	-842.1029	103.7
39	44231.0680	42109.0220	-2122.0460	-2222.5504	104.7
41	7349.5330	6999.9927	-349.5403	360.6076	103.2
42	6920.5279	6531.4016	-389.1263	-404.7290	104.0
44	5998.6512	5844.9335	-153.7177	-165.1199	107.4
45	5762.5105	5630.1473	-132.3632	-142.4745	107.6
47	7016.8980	6905.9260	-110.9720	-115.6099	104.2
48	6822.9614	6736.9477	-86.0137	-90.5011	105.2
50	9706.9951	9449.8267	-257.1684	-262.1729	102.0
51	9639.7495	9411.8005	-227.9490	-228.3732	100.2
53	13634.1000	12964.2560	-669.8440	-701.6882	104.8

Table 8.1 Continued

54	19874.8650	18390.3600	-1484.5050	-1586.2730	106.9
56	6080.3933	6078.1016	-2.2917	-3.6525	159.4
57	6121.4120	6114.6667	-6.7453	-8.1242	120.4
59	5832.8322	5697.4132	-135.4190	-139.1451	102.8
60	6266.5615	6098.1882	-168.3733	-172.9635	102.7
62	7041.7283	6971.4204	-70.3079	-79.6051	113.2
63	8230.6127	8059.7990	-170.8137	-188.3943	110.3
65	4816.1908	4793.3159	-22.8749	-24.1961	105.8
66	4787.5653	4761.5085	-26.0568	-27.6278	106.0
68	3537.2024	3578.9546	41.7522	40.3578	96.7
69	3692.9881	3725.9600	32.9719	31.0383	94.1
71	6541.8233	6585.9308	44.1075	45.1422	102.4
72	6643.3182	6680.1317	36.8135	38.0789	103.4
74	3872.7605	3898.8240	26.0635	25.4267	97.6
75	3820.6962	3843.9362	23.2400	22.5210	96.9
77	3918.9608	4017.5877	98.6269	100.0753	101.5
78	3932.8001	4024.4881	91.6880	92.9458	101.4
80	6240.3854	6285.3485	44.9631	46.3209	103.0
81	6158.4620	6202.3951	43.9331	45.2521	103.0

9. DESIGN COMPONENT METHOD FOR BUILT-UP STRUCTURES

In this section, design sensitivity analysis method for built-up structures is presented. Both shape and conventional (sizing) design variables for components of built-up structures are considered. For conventional design sensitivity analysis, distributed parameter structural design sensitivity analysis theory of Ref. 2 is used.

Consider a built-up structure that is made up of $m > 1$ structural components that are interconnected by kinematic constraints at their interfaces. Using the principle of virtual work for built-up structures [2], one can obtain the variational formulation of the governing equations,

$$a_{u,\Omega}(z,\bar{z}) = \ell_{u,\Omega}(\bar{z}), \qquad \text{for all } \bar{z} \in Z \tag{9.1}$$

where

$$a_{u,\Omega}(z,\bar{z}) = \sum_{i=1}^{m} a_{u^i,\Omega^i}(z,\bar{z}) \tag{9.2}$$

$$\ell_{u,\Omega}(\bar{z}) = \sum_{i=1}^{m} \ell_{u^i,\Omega^i}(\bar{z}) \tag{9.3}$$

and Z is the space of kinematically admissible displacements [2], which is defined as the set of displacement fields that satisfy homogeneous boundary conditions and kinematic interface conditions between components. In Eqs. 9.2 and 9.3, $a_{u^i,\Omega^i}(z,\bar{z})$ and $\ell_{u^i,\Omega^i}(\bar{z})$ are energy bilinear and load linear forms of component i with domain Ω^i. Note from Eqs. 9.2 and 9.3, the energy bilinear and load linear forms of Eq. 9.1 are simply summations of corresponding terms from each component. Thus, as will be seen later, the design sensitivity analysis of the built-up structure is a simple additive process.

In this section, design sensitivity information for displacement functional is derived for general built-up structures. Once this is done, extention to locally averaged stress functional can be carried out easily.

Define $\dot{z}$ as the total variation of z, due to both conventional and shape design changes [2],

$$\dot{z} = \frac{d}{d\tau} z_\tau(x+\tau V(x),\ u+\tau\delta u)\Big|_{\tau=0}$$
$$= \frac{d}{d\tau} z(x,u+\tau\delta u)\Big|_{\tau=0} + \frac{d}{d\tau} z_\tau(x+\tau V(x),u)\Big|_{\tau=0} \qquad [9.4]$$

The first variation of Eq. 9.1 is [2]

$$a'_{\delta u,\Omega}(z,\bar{z}) + a'_{u,V}(z,\bar{z}) + a_{u,\Omega}(\dot{z},\bar{z}) = \ell'_{\delta u,\Omega}(\bar{z}) + \ell'_{u,V}(\bar{z}),\ \text{for all } \bar{z}\in Z \qquad [9.5]$$

where $\dot{z} = [\dot{w}^1,\ \dot{w}^2,\ \dot{\theta},\ \dot{v}]^T$ for beam/truss component, $\dot{z} = [\dot{z}^1,\ \dot{z}^2,\ \dot{z}^3]^T$ for, three dimensional elastic solid, and $\dot{z} = [\dot{w},\ \dot{v}^1,\ \dot{v}^2]^T$ for plate/plane elastic solid component. The notation of Eq. 9.5 is chosen to clearly display which variables are held fixed and which vary.

Consider a displacement functional that defines the displacement z at nodal point $\hat{x}\in\Omega^r$

$$\psi = \int\!\!\int_{\Omega^r} \hat{\delta}(x-\hat{x})z(x)\ d\Omega \qquad [9.6]$$

where $\hat{\delta}(x)$ is the Dirac delta measure at the origin. Taking the first variation of Eq. 9.6, one obtains [2]

$$\psi' = \int\!\!\int_{\Omega^r} \hat{\delta}(x-\hat{x})\dot{z}(x)\ d\Omega \qquad [9.7]$$

Define a variational adjoint equation by replacing $\dot{z}$ in the term on the right of Eq. 9.7 by a virtual displacement $\bar{\lambda}$ and equate the result to the energy bilinear form evaluated at the adjoint variable λ; i.e.,

$$a_{u,\Omega}(\lambda,\bar{\lambda}) = \int\int_{\Omega^r} \hat{\delta}(x-\hat{x})\bar{\lambda}(x)\, d\Omega, \qquad \text{for all } \bar{\lambda} \in Z \qquad [9.8]$$

Denote the solution of Eq. 9.8 as λ. Since $\dot{z}$ satisfies kinematic boundary and interface conditions [2], Eq. 9.8 can be evaluated at $\bar{\lambda} = \dot{z}$ and Eq. 9.5 can be evaluated at $\bar{z} = \lambda$, to obtain

$$\psi' = \sum_{i=1}^{m} \left[\ell'_{\delta u^i,\Omega^i}(\lambda) - a'_{\delta u^i,\Omega^i}(z,\lambda) \right] + \sum_{i=1}^{m} \left[\ell'_{u^i,V^i}(\lambda) - a'_{u^i,V^i}(z,\lambda) \right] \qquad [9.9]$$

where the first term on the right is due to conventional design variation and the second term is due to shape design variation. Note that Eq. 9.9 is valid for general built-up structures that are composed of $m > 1$ structural components. For explicit expressions of the second term on the right of Eq. 9.9, results of Eqs. 5.1, 5.2, 5.4, and 5.7 - 5.9 can be used. For the first term on the right of Eq. 9.9, the interested reader is referred to Refs. 2 and 18.

As seen in this derivation, one can systematically organize design sensitivity expressions for built-up structures, using the design component method. Moreover, one can develop a modular computer program that will carry out numerical integration of terms in Eqs. 5.1, 5.2, 5.4, and 5.7 - 5.9, using the same shape functions that are employed by the finite element analysis of the original structure. The result will then be a general algorithm and numerical method for design sensitivity analysis that can be implemented with existing finite element codes as shown in Section 6.

To demonstrate accuracy of the design component method, a truss-beam-plate built-up structure is treated in this section. Consider the truss-beam-plate built-up structure shown in Fig. 9.1. A distributed vertical load $f(x)$ is applied to the plates. The points supported by the trusses are at the intersections of two crossing beams nearest to the free edges of the structure. No external loads are applied to the truss and beam components. The plates and beams are assumed to be welded together.

Coordinates of intersection points of beams and plates are supposed to be in the mid-planes of the plates and neutral axes of the beams. Beam components have rectangular cross-sections.

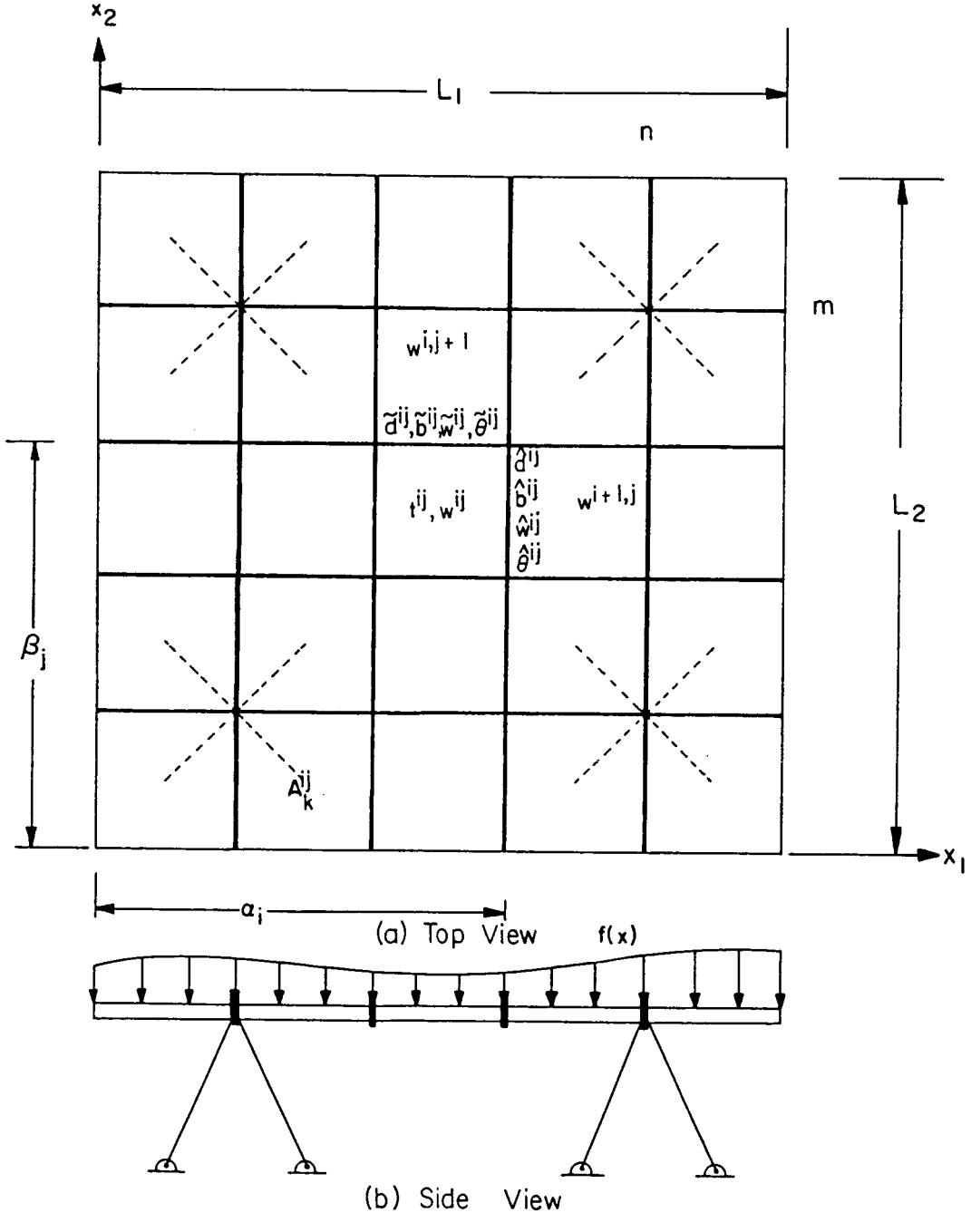

Figure 9.1 Truss-Beam-Plate Built-up Structure

The design variables for this built-up structure are thickness $t^{ij}(x)$ of each plate component, width $\tilde{d}^{ij}(x_1)$ and height $\tilde{b}^{ij}(x_1)$ of each longitudinal beam compoenent, width $d^{ij}(x_2)$ and height $b^{ij}(x_2)$ of each transverse beam component, cross-sectional areas h^k (k=1,16) of the four 4-bar truss components, and positions α_i (i=1,4) and β_j (j=1,4) of transverse and longitudinal beam components, respectively. The lengths of the trusses are fixed, but they may change their ground positions, and the outside boundary of the entire structure is fixed; i.e., only the locations α_i and β_j, i,j=1,4, of beams are shape variables. Dimensions of the structure and the numbering and spacing of beams in both directions are shown in Fig. 9.1.

For numerical calculations, conventional and shape design sensitivity calculations are carried out seperately. For plate components, 12 degree-of-freedom non-conforming rectangular elements [27] are used. For beam components, Hermite cubic shape functions are used. The finite element model used for design sensitivity analysis is shown in Fig. 9.2. Only one quarter of the entire structure is analyzed, due to symmetry. A total of 484 elements, with 1281 degrees-of-freedom, are used to model the built-up structure, including 400 rectangular plate elements, 80 beam elements and 4 truss elements.

For numerical data, Young's modulus and Poisson's ratio are 3.0×10^7 psi and 0.3, respectively. The overall dimensions are $L_1 \times L_2$ = 15 in. x 15 in. At the nominal design, beam components are located 3 in. apart. Other dimensions of the built-up structure at the nominal design are; uniform thickness t = 0.1 in. for plate components, uniform height h = 0.5 in. and width d = 0.15 in. for beam components, and length ℓ = 5.364 in. and cross-sectional area h = 0.1 $in.^2$ for truss components. A uniform distributed load f = 0.1 $lb/in.^2$ is applied on the plate components.

In Table 9.1, design sensitivity accuracy results are given for several functionals, with 1% uniform change in all conventional design variables except the cross-sectional areas of truss components. Design sensitivity results for displacements, bending stresses σ^{11} and σ^{22} at the extreme fiber of longitudinal and transverse beam components, and von Mises yield stress

$$g(\sigma) = (\sigma^{11^2} + \sigma^{22^2} + 3\sigma^{12^2} - \sigma^{11}\sigma^{22})^{1/2} \qquad [9.10]$$

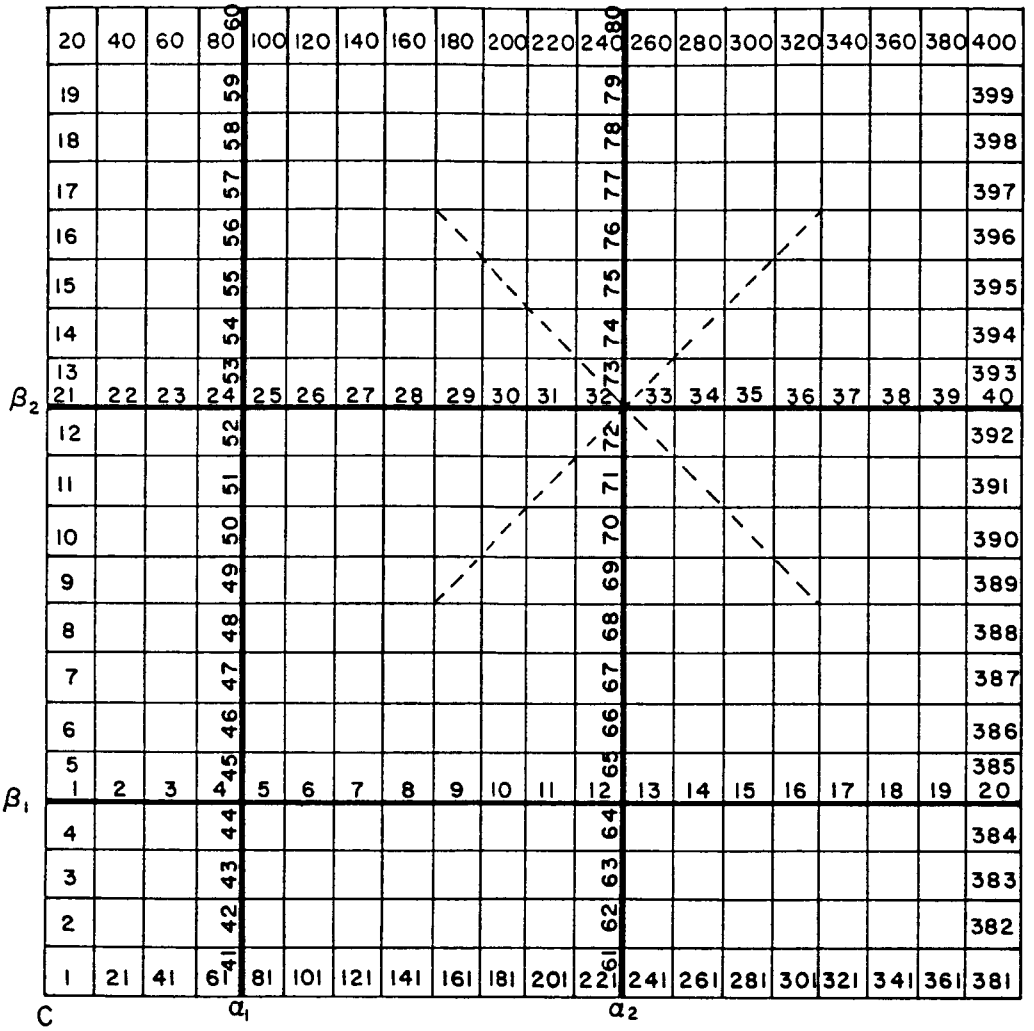

Figure 9.2 Finite Element Model of A Truss-Beam-Plate Built-up Structure

at the extreme fiber of plate components are given in Table 9.1. Results given in Table 9.1 show good agreement between predictions ψ' and finite differences $\Delta\psi$ except for von Mises yield stresses on plate elements 177, 358, 380 and 400 which are acceptable but not good. However, note that these elements have low von Mises yield stress and $\Delta\psi$ is small, compared to others, and may not be accurate.

For shape design sensitivity calculations, since the built-up structure is symmetric with respect to the center C, the locations α_i and β_j, i,j=1,2, of transverse and longitudinal beams, measured from the center C, are taken as design variables.

Table 9.1. Conventional Design Sensitivity of Truss-Beam-Plate Built-Up Structure

(a) Displacement

Node No.	ψ^1	ψ^2	$\Delta\psi$	ψ'	$(\psi'/\Delta\psi \times 100)\%$
53	-2.9755E-04	-2.8723E-04	1.0315E-05	9.5761E-06	92.8
95	-2.5890E-04	-2.4993E-04	8.9703E-06	8.3204E-06	92.8
113	-2.2837E-04	-2.2048E-04	7.8934E-06	7.3284E-06	92.8
137	-4.2898E-04	-4.1320E-04	1.5781E-05	1.6171E-05	102.5
179	-4.0427E-04	-3.8949E-04	1.4788E-05	1.5042E-05	101.7
221	-3.7551E-04	-3.6186E-04	1.3649E-05	1.3747E-05	100.7
268	-1.2025E-04	-1.1601E-04	4.2443E-06	4.1932E-06	98.8
310	1.4419E-05	1.3799E-05	-6.1962E-07	-6.1013E-07	98.5
335	1.5392E-04	1.4824E-04	-5.6883E-06	-5.3932E-06	94.8
352	5.5382E-05	5.3329E-05	-2.0534E-06	-1.9995E-06	97.4

(b) Bending Stress on Beam Element

El. No.	ψ^1	ψ^2	$\Delta\psi$	ψ'	$(\psi'/\Delta\psi \times 100)\%$
1	160.415	155.757	-4.658	-5.250	112.7
4	128.072	124.347	-3.725	-4.271	114.7
21	365.447	355.610	-9.837	-9.608	97.7
25	305.855	297.648	-8.207	-8.191	99.8
30	-69.361	-67.350	2.011	2.233	111.0
45	106.547	103.409	-3.138	-3.383	107.8
49	24.570	23.801	-0.769	-0.963	125.2
54	-74.026	-72.026	2.000	2.141	107.1
60	-4.789	-4.624	0.165	0.162	98.0
80	2.141	2.063	-0.079	-0.080	102.1

(c) von Mises Stress on Plate Element

El. No.	ψ^1	ψ^2	$\Delta\psi$	ψ'	$(\psi'/\Delta\psi \times 100)\%$
1	49.128	47.808	-1.320	-1.560	118.2
5	34.279	33.323	-0.956	-1.059	110.8
9	62.143	60.507	-1.636	-1.695	103.6
13	77.076	75.067	-2.009	-1.982	98.6
17	92.755	90.404	-2.351	-2.157	91.7
22	44.262	43.040	-1.222	-1.459	119.4

Table 9.1(c) Continued

26	42.663	41.471	-1.192	-1.247	104.6
30	63.522	61.831	-1.691	-1.729	102.2
34	77.930	75.877	-2.053	-1.946	94.8
38	91.868	89.533	-2.335	-2.105	90.1
44	33.332	32.332	-1.000	-1.189	118.9
48	52.498	51.074	-1.424	-1.477	103.8
52	67.527	65.707	-1.820	-1.761	96.7
56	79.045	76.974	-2.071	-1.895	91.0
65	38.362	37.273	-1.090	-1.150	105.5
69	46.061	44.733	-1.328	-1.297	97.7
73	70.749	68.874	-1.875	-1.784	95.2
77	67.127	65.280	-1.847	-1.609	87.1
85	38.300	37.201	-1.099	-1.104	100.5
89	47.855	46.506	-1.348	-1.288	95.6
93	67.866	66.083	-1.783	-1.759	98.7
97	62.719	61.070	-1.649	-1.602	97.2
106	43.048	41.825	-1.223	-1.191	97.4
112	62.228	60.640	-1.588	-1.477	93.0
118	59.270	57.835	-1.435	-1.385	96.5
128	55.122	53.691	-1.431	-1.362	95.1
134	48.012	46.800	-1.211	-1.119	92.4
140	56.823	55.539	-1.284	-1.214	94.5
151	53.218	51.887	-1.331	-1.183	88.9
155	37.003	36.148	-0.855	-0.735	85.9
159	37.897	37.097	-0.800	-0.691	86.4
169	52.077	50.777	-1.300	-1.163	89.5
173	56.294	54.890	-1.404	-1.292	92.0
177	23.383	22.944	-0.439	-0.276	62.8
192	61.326	59.720	-1.605	-1.568	97.7
198	27.041	26.479	-0.562	-0.451	80.3
212	67.683	65.843	-1.840	-1.854	100.8
216	53.350	52.077	-1.273	-1.264	99.3
235	82.704	80.664	-2.041	-2.127	104.2
239	100.980	98.872	-2.107	-2.104	99.8
255	79.509	77.476	-2.033	-1.968	96.8
259	101.657	99.539	-2.117	-2.040	96.4
274	67.361	65.559	-1.802	-1.765	98.0
278	64.853	63.399	-1.454	-1.403	96.5
288	37.003	36.148	-0.855	-0.735	85.9
319	27.894	27.305	-0.590	-0.586	99.4
337	21.848	21.459	-0.389	-0.419	107.6
358	14.556	14.427	-0.129	-0.190	146.8
380	12.189	12.077	-0.113	-0.161	142.8
400	8.471	8.381	-0.090	-0.119	132.8

As mentioned in Section 8, for shape design sensitivity calculations, one must define a velocity field that has C^1-regularity with its second derivative integrable. The beam components are allowed to move in transverse directions only. Hence, V^1 is a function of x_1 only and V^2 is a function of x_2 only. The velocity field in each plate component is

represented by Hermite cubic functions in each direction. That is, $V^1(x_1)$ and $V^2(x_2)$ are represented by Hermite cubic functions. To see the velocity field representation graphically, consider Fig. 9.3, in which the shape functions for $V^1(x_1)$ are plotted. In Fig. 9.3, $\delta\alpha_1$ and $\delta\alpha_2$ denote perturbations of locations of transverse beams. From Fig. 9.3, one obtains $V^1(x_1) = \phi^1(x_1) + \phi^2(x_1)$. That is,

$$V^1(x_1) = \begin{cases} -\dfrac{2x^2}{\alpha_1^3}\left(x - \dfrac{3\alpha_1}{2}\right)\delta\alpha_1, & 0 \leq x \leq \alpha_1 \\ \dfrac{2(x-\alpha_1)^2}{(\alpha_2-\alpha_1)^3}\left[(x-\alpha_1) - \dfrac{3(\alpha_2-\alpha_1)}{2}\right](\delta\alpha_1-\delta\alpha_2) + \delta\alpha_1, & \alpha_1 \leq x \leq \alpha_2 \\ \dfrac{2(x-\alpha_2)^2}{\left(\frac{L_1}{2}-\alpha_2\right)^3}\left[(x-\alpha_2) - \dfrac{3\left(\frac{L_1}{2}-\alpha_2\right)}{2}\right]\delta\alpha_2 + \delta\alpha_2, & \alpha_2 \leq x \leq \dfrac{L_1}{2} \end{cases} \quad [9.11]$$

and a similar expression for $V^2(x_2)$.

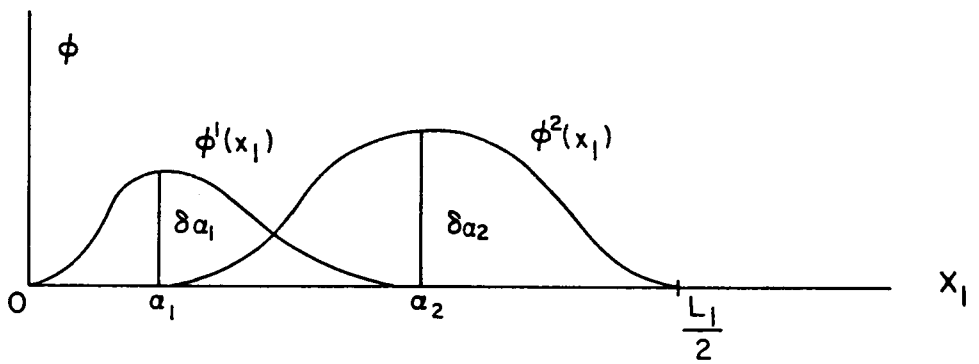

Figure 9.3 Shape Functions For The Velocity $V^1(x_1)$

In Table 9.2, design sensitivity accuracy results are given for several functionals, with a 0.25% uniform change in shape design parameters. Sensitivity results for displacements, bending stress for beam components, and von Mises yield stress for plate components, are given in Table 9.2. Results given in Table 9.2 show excellent agreement between predictions ψ' and the finite differences $\Delta\psi$.

Table 9.2. Shape Design Sensitivity of Truss-Beam-Plate Built-Up Structure

(a) Displacement

Node No.	ψ^1	ψ^2	$\Delta\psi$	ψ'	$(\psi'/\Delta\psi \times 100)\%$
53	-2.9755E-04	-3.0123E-04	-3.6843E-06	-3.6386E-06	98.8
95	-2.5890E-04	-2.6186E-04	-2.9640E-06	-2.9212E-06	98.6
113	-2.2837E-04	-2.3080E-04	-2.4214E-06	-2.3798E-06	98.3
137	-4.2898E-04	-4.3951E-04	-1.0535E-05	-1.0489E-05	99.6
179	-4.0427E-04	-4.1394E-04	-9.6675E-06	-9.6264E-06	99.6
221	-3.7551E-04	-3.8411E-04	-8.5986E-06	-8.5631E-06	99.6
268	-1.2025E-04	-1.2319E-04	-2.9391E-06	-2.9273E-06	99.6
310	1.4419E-05	1.5210E-05	7.9096E-07	7.9419E-07	100.4
335	1.5392E-04	1.5978E-04	5.8589E-06	5.8686E-06	100.2
352	5.5382E-05	5.7951E-05	2.5690E-06	2.5786E-06	100.4

(b) Bending Stress on Beam Element

El. No.	ψ^1	ψ^2	$\Delta\psi$	ψ'	$(\psi'/\Delta\psi \times 100)\%$
1	160.415	163.634	3.219	3.095	96.2
4	128.072	131.041	2.968	2.871	96.7
21	365.447	370.311	4.864	4.586	94.3
25	305.855	310.385	4.530	4.399	97.1
30	-69.361	-66.654	2.708	2.820	104.2
45	106.547	109.385	2.838	2.794	98.4
49	24.570	26.757	2.187	2.143	98.0
54	-74.026	-73.243	0.783	0.663	84.7
60	-4.789	-4.853	-0.064	-0.065	101.8
80	2.141	2.113	-0.028	-0.026	91.2

(c) von Mises Stress on Plate Element

El. No.	ψ^1	ψ^2	$\Delta\psi$	ψ'	$(\psi'/\Delta\psi \times 100)\%$
1	49.128	50.043	0.915	0.915	100.1
5	31.279	34.881	0.602	0.600	99.6
9	62.143	63.067	0.925	0.924	99.9
13	77.076	77.949	0.873	0.871	99.8
17	92.755	93.843	1.088	1.090	100.2
22	44.262	45.153	0.891	0.891	100.0

Table 9.2(c) Continued

26	42.663	43.440	0.778	0.776	99.8
30	63.522	64.437	0.914	0.913	99.8
34	77.930	78.891	0.961	0.960	99.9
38	91.868	93.039	1.171	1.172	100.1
44	33.332	34.143	0.811	0.810	99.9
48	52.498	53.329	0.831	0.830	99.9
52	67.527	68.410	0.883	0.881	99.7
56	79.045	80.149	1.104	1.104	100.0
65	38.362	39.116	0.754	0.749	99.4
69	46.061	46.804	0.743	0.742	99.9
73	70.749	71.663	0.914	0.911	99.7
77	67.127	68.334	1.207	1.209	100.1
85	38.300	39.039	0.740	0.738	99.8
89	47.855	48.520	0.665	0.663	99.7
93	67.866	68.758	0.892	0.889	99.6
97	62.719	64.012	1.293	1.294	100.1
106	43.048	43.773	0.726	0.725	99.9
112	62.228	62.978	0.749	0.745	99.3
118	59.270	60.553	1.283	1.284	100.1
128	55.122	55.881	0.759	0.756	99.7
134	48.012	48.846	0.834	0.830	99.4
140	56.823	58.228	1.405	1.408	100.2
151	53.218	53.793	0.575	0.569	99.0
155	37.003	37.871	0.868	0.863	99.4
159	37.897	39.123	1.226	1.226	100.0
169	52.077	52.764	0.687	0.683	99.3
173	56.294	56.509	0.215	0.208	96.7
177	23.383	24.298	0.915	0.907	99.1
192	61.326	61.258	-0.068	-0.075	109.9
198	27.041	27.324	0.283	0.263	93.0
212	67.683	67.463	-0.220	-0.226	102.7
216	53.350	53.241	-0.109	-0.118	107.7
235	82.704	82.424	-0.280	-0.285	101.6
239	100.980	101.057	0.077	0.075	97.5
255	79.509	79.143	-0.366	-0.369	100.9
259	101.657	101.295	-0.362	-0.364	100.6
274	67.361	66.997	-0.364	-0.368	101.2
278	64.853	64.565	-0.288	-0.290	100.7
288	37.003	37.871	0.868	0.863	99.4
319	27.894	27.717	-0.177	-0.182	102.5
337	21.848	21.623	-0.225	-0.230	102.2
358	14.556	14.247	-0.309	-0.313	101.2
380	12.189	11.934	-0.255	-0.255	100.1
400	8.471	8.315	-0.156	-0.154	99.1

10. AN OPTIMIZATION PROBLEM

To demonstrate application of the design sensitivity analysis method for built-up structures in structural design optimization, the truss-beam-

plate built-up structure of Section 9 is optimized using a sparse matrix symbolic factorization technique for iterative structural optimization [28] and Pshenichny's linearization method [29].

For numerical design sensitivity analysis and optimization, design variables are discretized. That is, each plate element has constant thickness and each beam element has constant width and height. Since the built-up structure is symmetric with respect to the center C, thickness t_i, i = 1,210, width d_i and height b_i, i = 1, 40, and the locations α_i, i = 1, 2 of transverse and longitudinal beams, measured from the center C, are taken as design parameters. Thus, the total number of design parameters is 292.

The optimal design problem of the built-up structure is to minimize weight of the structure, subject to the following constraints:

Displacement at C; $\psi_1 = z(C) \leq 0.105$ in.

Plate element von Mises stress; $\psi_i \leq 17500$ psi, i = 2,211

Beam element bending stress; $-70000 \text{ psi} \leq \psi_i \leq 70000$ psi, i = 212,251

Plate thickness; $0.05 \text{ in.} \leq t_i \leq 0.25$ in., i = 1,210

Beam width; $0.075 \text{ in.} \leq d_i \leq 0.30$ in., i = 1, 40

Beam height; $0.25 \text{ in.} \leq b_i \leq 1.00$ in., i = 1, 40

Beam position; $0 \leq \alpha_1 \leq \alpha_2 \leq \frac{L_1}{2}$

Thus, the total number of inequality constraints is 543.

Same numerical data as in Section 9 is used except weight density is 0.1 lb/in.^{3} and uniformly distributed load f = 17.5 lb/in.^{2} is applied to the plate components.

For numerical computation of the shape design sensitivity information, derivatives I_x, J_x, and h_x in Eq. 5.1 for beam component and ∇t in Eq. 5.8 for plate component must be computed. Since each plate element has constant thickness and each beam element has constant width and height, these derivatives are Dirac delta measures and computations of the shape design sensitivity information become complicated.

To avoid this difficulty, the design process is divided into two phases. In Phase I, each plate and beam components (not element) have constant thickness and constant width and height, respectively. Hence in Phase I, the design parameter set includes 6 plate thicknesses, 6 beam heights and widths, and 2 beam locations with total of 20 design parameters. To assign the same design parameter to elements in a component, design variable linking is used in Phase I. Once an optimum

point is reached in Phase I, the design process is switched to Phase II where shape design parameters are fixed and each plate and beam elements are allowed to have different design parameters. Hence the total number of design parameter is 290 in Phase II.

For numerical computation, PRIME-750 and Cray-1S computers are used for design Phases I and II, respectively. The initial and final designs of Phase I is given in Table 10.1. The initial cost is 0.7875 lb and the final cost of Phase I is 0.5894 lb. There are 12 design iterations in

Table 10.1. Initial and Final Designs of Phase I

Design Parameter		Initial Design	Final Design
Plate Component Thickness	t_1	0.1	0.0874
	t_2		0.0500
	t_3		0.0518
	t_4		0.0501
	t_5		0.0815
	t_6		0.0910
Beam Component Height	b_1	0.5	0.4234
	b_2		0.6902
	b_3		0.4990
	b_4		0.3974
	b_5		0.4266
	b_6		0.4326
Beam Component Width	d_1	0.15	0.1087
	d_2		0.2214
	d_3		0.2499
	d_4		0.0754
	d_5		0.0838
	d_6		0.1286
Beam Position	α_1	1.50	1.4221
	α_2	4.50	4.5872

Phase I with average CPU time 15986 seconds per iteration on a PRIME-750 computer. It is observed in design Phase I that inner beam stiffners move inward (α_1 = 1.4211 in.) and outer beam stiffners move outward (α_2 = 4.5872 in.). Number of active stress and displacement constraints at the final design of Phase I is 31. Thus, it is necessary to calculate sensitivity information for 31 constraints out of 251.

There are 9 design iterations in Phase II with average CPU time 25.84 seconds per iteration on a Cray-1S computer. Cost function history of Phases I and II is shown in Fig. 10.1. The final cost of Phase II is 0.5388 lb. Number of active stress and displacement constraints at the final design of Phase II is 54. A profile of upper half of the final design is shown in Fig. 10.2

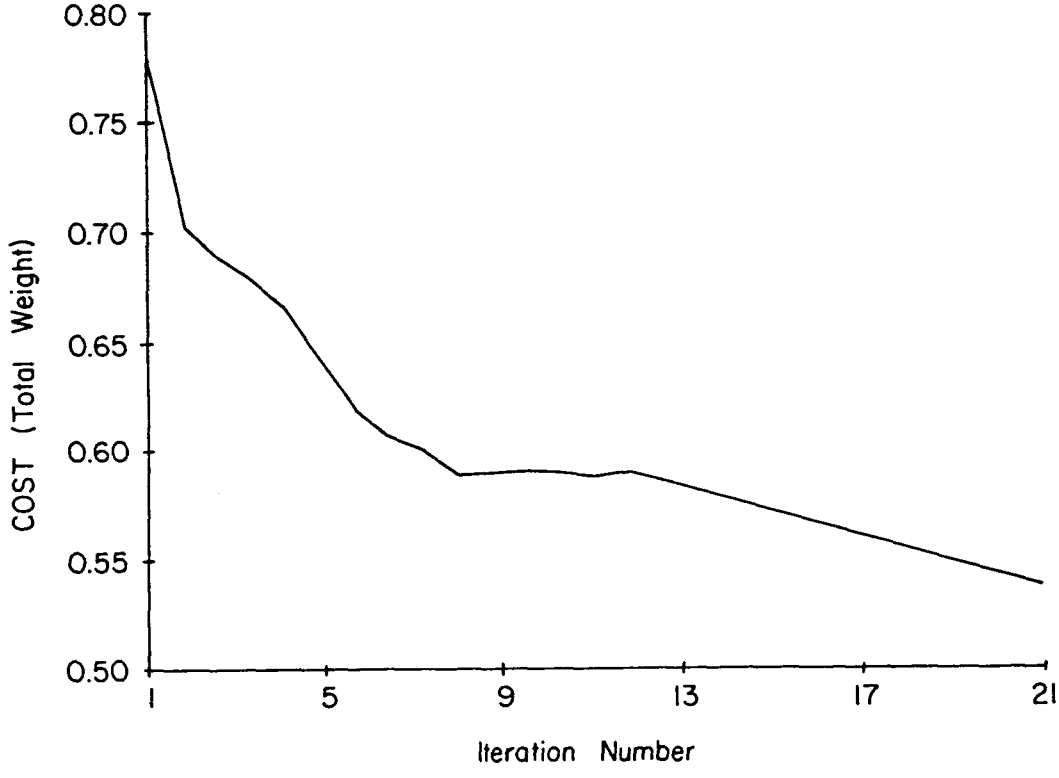

Figure 10.1 Cost Function History

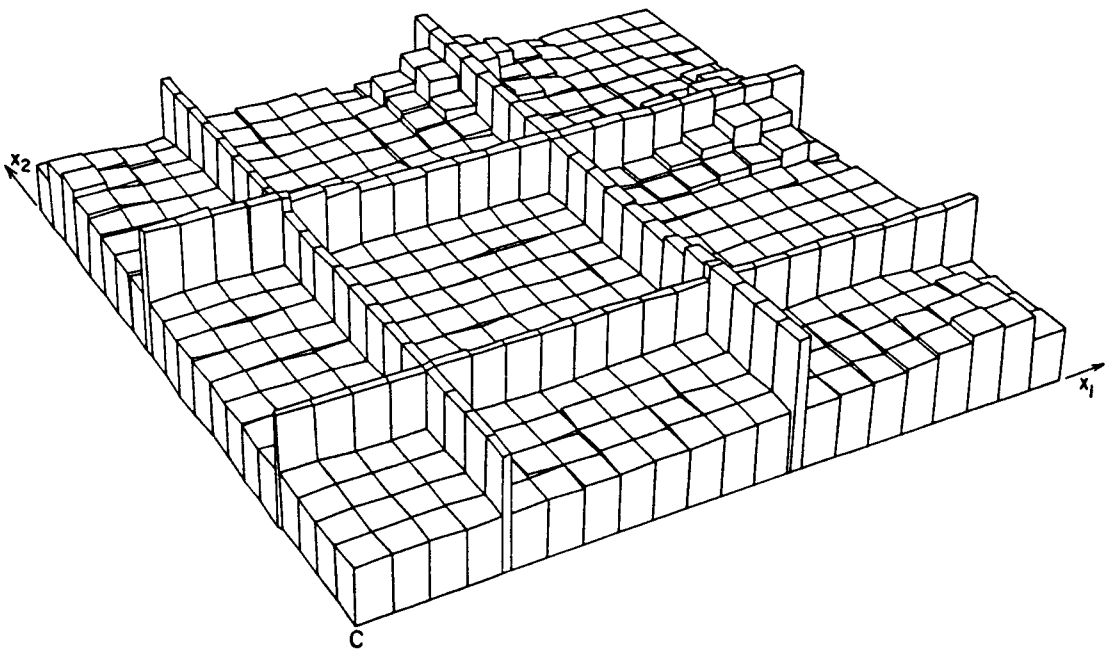

Figure 10.2 A Profile of the Final Design

REFERENCES

1. Haftka, R.T. and Kamat, M.P., Elements of Structural Optimization, Martinus Nijhoff Publishers, Boston, 1985.
2. Haug, E.J., Choi, K.K. and Komkov, V., Design Sensitivity Analysis of Structural Systems, Academic Press, New York, N.Y., March, 1986.
3. Haftka, R.T. and Grandhi, R.V., "Structural Shape Optimization-Survey," Computer Methods in Applied Mechanics and Engineering, to appear, 1986.
4. Botkin, M.E., "Shape Optimization of Plate and Shell Structures," AIAA J., Vol. 20, No. 2, 1982, pp. 268-273.
5. Francavilla, A., Ramakrishnan, C.V. and Zienkiewicz, O.C., "Optimization of Shape to Minimize Stress Concentration," J. of Strain Analysis, Vol. 10, No. 2, 1975, pp. 63-70.
6. Braibant, V. and Fleury, C., "Shape Optimal Design Using B-Splines," Computer Methods in Applied Mechanics and Engineering, Vol. 44, 1984, pp. 247-267.
7. Dems, K. and Mroz, Z., "Variational Approach by Means of Adjoint Systems to Structural Optimization and Sensitivity Analysis - II Structural Shape Variation," Int. J. Solids and Structures, Vol. 20, No. 6, 1984, pp. 527-552.
8. Cea, J. "Problems of Shape Optimal Design," Optimization of Distributed Parameter Structures, E.J. Haug and J. Cea (Eds.), Sijthoff & Noordhoff, Alpen ann den Rijn, The Netherlands, 1981, pp. 1005-1048.
9. Choi, K.K. and Haug, E.J., "Shape Design Sensitivity Analysis of Elastic Structures," J. of Struct. Mechanics, Vol. 11, No. 2, 1983, pp. 231-269.
10. Choi, K.K., "Shape Design Sensitivity Analysis of Displacement and Stress Constraints," J. of Struct. Mechanics, Vol. 13, No. 1, 1985, pp. 27-41.
11. Haug, E.J., Choi, K.K., Hou, J.W. and Yoo, Y.M., "A Variational Method for Shape Optimal Design of Elastic Structures," New Directions in Optimum Structural Design, E. Atrek, R.H. Gallagher, K.M. Ragsdell and O.C. Zienkiewicz (Eds.), John Wiley and Sons, Ltd., 1984, pp. 105-137.
12. Banichuk, N.V., "Optimization of Elastic Bars in Torsion," Int. J. of Solids and Structures, Vol. 12, 1976, pp. 275-286.
13. Na, M.S., Kikuchi, N. and Taylor, J.E., "Shape Optimization for Elastic Torsion Bars," Optimization Methods in Structural Design, H. Eschenauer and N. Olhoff (Eds.), Bibliographisches Institut, Zurich, Germany, 1983, pp. 216-223.
14. Babuska, I. and Aziz, A.K., "Survey Lectures on the Mathematical Foundations of the Finite Element Method," The Mathematical Foundations of the Finite Element Method with Applications to Partial Differential Equations, Academic Press, 1972, pp. 1-359.
15. Choi, K.K. and Seong, H.G., "A Domain Method for Shape Design Sensitivity Analysis of Built-Up Structures," Computer Methods in Applied Mechanics and Engineering, to appear, 1986.
16. Seong, H.G. and Choi, K.K., "Boundary Layer Approach to Shape Design Sensitivity Analysis," J. of Struct. Mechanics, to appear, 1986.
17. Choi, K.K. and Yao, T.M., "3-D Modeling and Automatic Regridding in Shape Design Sensitivity Analysis," NASA Symposium: Sensitivity Analysis in Engieering, NASA-Langley Research Center, Virginia, September 25-26, 1986.

18. Choi, K.K. and Seong, H.G., "Design Component Method for Sensitivity Analysis of Built-Up Structures," J. of Struct. Mechanics, to appear, 1986.
19. Choi, K.K., Santos, J.L.T., and Frederick, M.C., "Implementation of Design Sensitivity Analysis with Existing Finite Element Codes," ASME Journal of Mechanisms, Transmissions, and Automation in Design, 85-DET-77.
20. Zolesio, J-P., "The Material Derivative (or Speed) Method for Shape Optimization," Optimization of distributed Parameter Structures, E.J. Haug and J. Cea (Eds.) Sijthoff & Noordhoff, Alphen ann den Rijn, The Netherlands, 1981, pp. 1089-1151.
21. Zolesio, J-P., "Gradient des coute Governes par des Problems de Neumann
poses des Wuverts Anguleux en Optimization de Domain, CRMA-Report 116, University of Montreal, Canada, 1982.
22. Choi, K.K. and Seong, H.G., "A Numerical Method for Shape Design Sensitivity Analysis and Optimization of Built-Up Structures," The Optimum Shape: Automated Structural Design, (Eds. J.A. Bennett and M.E. Botkin), Plenum Press, New York, 1986.
23. Yang, R.J. and Choi, K.K., "Accuracy of Finite Element Based Design Sensitivity Analysis," J. of Struct. Mechanics, Vol. 13, No. 2, 1985, pp. 223-239.
24. Dym, C. and Shames, I.H., Solid Mechanics-A Variational Approach, McGraw-Hill, 1973.
25. Rogers, D.F. and Adams, J.A., Mathematical Elements for Computer Graphics, McGraw-Hill, 1976.
26. DeSalvo, G.J. and Swanson, J.A., ANSYS Engineering Analysis System, Users Manual, Swanson Analysis System, Inc., P.O. Box 65, Houston, PA, Vols. I and II, 1983.
27. Przemieniecki, J.S., Theory of Matrix Structural Analysis, McGraw-Hill, 1968.
28. Lam, H.L., Choi, K.K., and Haug, E.J., "A Sparse Matrix Finite Element Technique for Iterative Structure Optimization," Computers and Structures, Vol. 16, No. 1-4, 1983, pp. 289-295.
29. Choi, K.K., Haug, E.J., Hou, J.W., and Sohoni, V.N., "Pshenichny's Linearization Method for Mechanical System Optimization," ASME Journal of Mechanisms, Transmissions, and Automation in Design, Vol. 105, No. 1, 1983, pp. 97-103.